Science of the Total Environment 918 (2024) 170315

Contents lists available at ScienceDirect

Science of the Total Environment

journal homepage: www.elsevier.com/locate/scitotenv

Aerosol characterization and peculiarities of source apportionment in Moscow, the largest and northernmost European megacity

Olga Popovicheva [a,*], Evangelia Diapouli [b], Marina Chichaeva [c], Natalia Kosheleva [c], Roman Kovach [c], Viktoria Bitukova [c], Konstantinos Eleftheriadis [b], Nikolay Kasimov [c]

[a] Scobeltsyn Institute of Nuclear Physics, Lomonosov Moscow State University, Moscow 119991, Russia
[b] Institute of Nuclear & Radiological Sciences & Technology, Energy & Safety, N.C.S.R. "Demokritos", Athens 15310, Greece
[c] Faculty of Geography, Lomonosov Moscow State University, Moscow 119991, Russia

HIGHLIGHTS

- Aerosol characterization and source apportionment is firstly performed for Moscow megacity
- Northern climate, gas-fueled heating, fast construction, winter road management imposes peculiarities among large cities
- PM10 mass approaches maximum in spring, SIA in opposite in cold seasons
- City dust factor dominates, in spring 52%.
- Regional residential heating/agriculture fires impact BB factor maximum in spring/autumn and minimum in winter

GRAPHICAL ABSTRACT

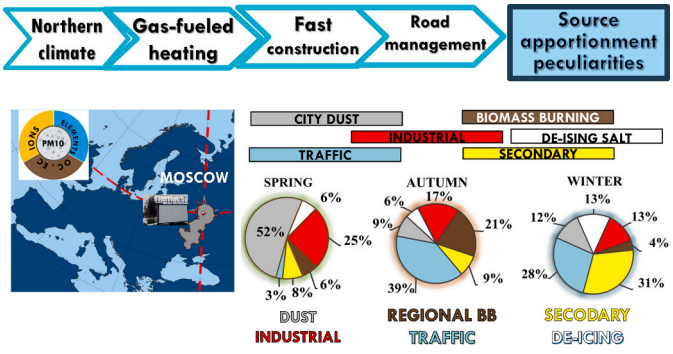

ARTICLE INFO

Editor: Jianmin Chen

Keywords:
Air pollution
City dust
Traffic
Secondary
Biomass burning
De-icing

ABSTRACT

High population and a wide range of activities in a megacity lead to large-scale ecological consequences which require the assessment with respect to distinct characteristics of climate, location, fuel consumption, and emission sources. In-depth study of aerosol characteristics was carried out in Moscow, the largest megacity in Europe, during the cold period (autumn and winter) and in spring. PM_{10} chemical speciation based on carbonaceous matter, water-soluble ions, and elements was carried out to reconstruct the PM mass and evaluate the primary and secondary aerosol contribution. For the whole study period organic matter, mineral dust, and secondary inorganic/organic accounted for 34, 24, and 16 % of PM_{10} mass, respectively. PM10, OC, and EC approached a maximum in spring and decreased in winter. Mineral dust seasonal fraction increased from spring (17 %) to autumn (32 %), and then decreased in winter (22 %). Secondary inorganic aerosols (SIA) in opposite showed the maximum 27 % in winter. K^+ marked the residential biomass burning in the region surrounding a megacity in spring and autumn, agriculture fires in spring. In winter primary aerosol contribution dropped down 56 % while secondary approached practically equal 44 %. Source factors with the relative contributions are quantified, namely city dust (26 %), traffic (23 %), industrial (20 %), biomass burning (12 %), secondary (12 %), and de-icing salt (7 %); they were significantly varying between the cold heating period and springtime. The relevance of sources to meteorological parameters and mass transportation is investigated by using both bivariate

* Corresponding author.
E-mail address: olga.popovicheva@gmail.com (O. Popovicheva).

https://doi.org/10.1016/j.scitotenv.2024.170315
Received 27 September 2023; Received in revised form 15 January 2024; Accepted 18 January 2024
Available online 24 January 2024
0048-9697/© 2024 Elsevier B.V. All rights reserved.

polar plots and Lagrangian integrated trajectory (HYSPLIT) model. Trajectory clustering demonstrates regional sources being crucial contributors to PM_{10} pollution. Aerosol speciation and source apportion factors identify the differences of the Moscow urban background among large European and Asian cities due to northern climate conditions, fast construction, long-range transport from industrial-developing area surrounding a city, regional biomass burning preferably in spring and autumn, and winter road management.

1. Introduction

Particulate matter (PM) in the atmosphere may originate from a variety of sources responsible for their observed concentration levels. Development of effective approach for air pollution assessment is crucial for the protection of public health, especially in megacities, where high population density and various socioeconomic activities result in numerous emission sources. Chemical speciation of ambient PM coupled to receptor modeling is currently considered as one of the most powerful tools for this purpose (Karagulian and Belis, 2012; Viana et al., 2008).

Receptor-oriented source apportionment models are based on a principle that ambient chemical concentrations are expressed as the sum of products of species abundances in emissions and source contributions (Watson et al., 2008). Among the different receptor models, Positive Matrix Factorization (PMF) is the most frequently applied when sources are not a-priori known but it requires post-treatment source identification. PMF analysis use PM chemical composition data that allow to define the primary and secondary sources impacting a given receptor site. Among the key components serving as source tracers are organic carbon (OC) and elemental (EC) for combustion sources. Mineral dust is the major component of PM mass in the atmosphere (Alastuey et al., 2016). Whereas satellite observations suggest that the anthropogenic fraction of suspended mineral dust on the global scale represents only 20 to 25 % of the total (Ginoux et al., 2012), on local and regional scales its anthropogenic contribution can become the dominant source and so highly affect air quality (Querol et al., 2004). Trace elements such as Cu, Ba, Sb and Zn act as markers for non-exhaust emissions (brake and tire wear); industry (particular metallurgy) is identified by Cr, Ni, and Mn; Ni and V are useful tracers for heavy oil combustion (Alastuey et al., 2016). Industrial processing relates to Zn, Pb, Cu, Mn, and As (Watson et al., 2008). Potassium ion appears as a main marker for biomass burning (Nava et al., 2015). The impact of secondary aerosol formation is identified by sulfate, nitrate, and ammonium (Seinfeld and Pandis, 2016).

In a number of studies (Belis et al., 2013; Viana et al., 2008) sources of PM pollution identified by the PMF model for the urban background, traffic, and industrial sites in urban, suburban, residential, and remote areas include traffic, city dust, industry, secondary aerosol, and residential heating (biomass and coal burning). The contribution of sources such as soil resuspension, long-range transported dust, and wildfire plumes are evaluated (Diapouli et al., 2017b; Diapouli et al., 2014). Source region cluster analyses using air mass back trajectories complements the apportionment techniques giving a possibility to estimate the relative importance of regional sources (Molnár et al., 2017).

Many studies have been undertaken to assess the sources in areas where concentrations of PM exceed the limit values or where they are cause for concern of harmful health effects and detrimental environment impacts of atmospheric pollution (Gupta et al., 2012; Ma et al., 2022; Masiol et al., 2020; Perrone et al., 2018). A large number of source apportionment have been performed in urban centres in Europe, North America and South-Eastern Asia, demonstrating the similarities and differences among regions of the different climatic zones, level of industrialization, population density, and fuel consumption (Almeida et al., 2020; Amato et al., 2015; Diapouli et al., 2017a; Waked et al., 2014; Zhu et al., 2018). Assessment of pollution in global megacities, based on mass concentration and composition data indicated that the highly polluted megacities are concentrated in east-central China and the Indo - Gangetic Plain (Cheng et al., 2016). In a northern megacity the distinct climatological characteristics related to heating system operation, much fuel consumption and population activity make it an important issue for the assessment by advanced aerosol characterization.

Moscow is the largest northernmost megacity in Europe. In Moscow, mass concentrations of fine particulate matter with a diameter of <2.5 μm ($PM_{2.5}$) were found to be around 20–30 μg/m^3 in yearly average, comparable or slightly higher than in other big European cities and lower than in Asian megacities (50–100 μg/m^3) (Cheng et al., 2016). According to air quality characterization based on multi-pollutant index, Moscow is classified among the slightly polluted megacities in Europe and North America (Elansky et al., 2018). Black carbon (BC) measurements addressed the level of air pollution in the city is substantially lower than in Beijing (Golitsyn et al., 2015). In spring BC level was comparable to Helsinki city between other European cities (Järvi et al., 2008; Popovicheva et al., 2020a). Concerning ionic composition, there is no particularly critical issues found about atmospheric pollution in Moscow urban background, in comparison to evaluated large European and Canadian cities (Zappi et al., 2023).

Source apportionment is more important in the urban environment where exposure and hazard air pollution are sensibly higher, owing to the significant population density and related activities such as transport, industry, and heating etc. In this respect, megacities such as Moscow with over ten million inhabitants require a special focus, since emissions and consequent air quality standards might reveal even more unsafe for human health, material infrastructures as well as cultural heritage (Baklanov et al., 2020). Despite a number of distinct characteristics and sources different from European and Asian cities, comprehensive chemical characterization and source apportionment in the Moscow megacity is still lacking. The first PCA - based source apportionment in the urban background used OC, EC, organic compounds, and ions; it addressed the spring factors for marker species related to traffic, biomass burning, biogenic activity, and secondary formation in the atmosphere (Popovicheva et al., 2020b). BC level in the Moscow urban background (Popovicheva et al., 2020a) as well as in the Moscow center (Golitsyn et al., 2015) indicated a strong impact of transport. High frequencies of backward trajectories from the European part of Russia in the warm season confirmed the large agriculture and wildfires impact to the air pollution of a megacity (Popovicheva et al., 2020c, 2022; Zappi et al., 2023). The highest smoke events occurred in August of 2010 (Popovicheva et al., 2014) and 2014 (Popovicheva et al., 2019b). A systematical investigation of employing multiple techniques in conjunction with chemical measurements is inevitably needed for Moscow ambient aerosols, particularly to unravel the contributors of PM_{10} mass from traffic, and biomass burning, and regional sources.

The aim of the study is the comprehensive chemical characterization and sources apportionment of atmospheric fine particulate matter in the Moscow megacity. PM_{10} sampling campaign was carried out in spring 2018, autumn 2019, and winter 2019–2020 at the Moscow urban background site (Aerosol Complex MSU). The samples were subjected to measurements for aerosol components such as OC, EC, water-soluble ions, major and trace elements. We present the seasonal variation of aerosol composition and descriptive statistics, calculate the mass closure and estimate the contribution of primary and secondary aerosol species to PM_{10} mass. Furthermore, we identify and apportion the main sources of PM10 by employing the PMF model. The source profiles in spring, autumn, and winter, and the relative contribution from each source are presented. The relevance of the factors to meteorological parameters

and air mass transportation is investigated by using the both bivariant polar plots and the Lagrangian integrated trajectory (HYSPLIT) model. To address the spatial distribution of regional sources the trajectory clustering is employed. It should be noted that this is the first source apportionment study performed for the Moscow aerosol environment. Particularities of source apportionment for Moscow megacity are considered, demonstrating the similarities and differences among urban backgrounds of large European and Asian cities.

Fig. 1. (On top) Moscow megacity in the European part of Russia. Moscow city, Moscovskaya Oblast, and surrounding districts are in insert on the right. (On bottom) Moscow area with 150 stationary industrial enterprises indicated within 15 km around Meteorological Observatory of Moscow State University (MO MSU) (55° 42′ N; 37° 31′ E), types of production is indicated. Large highways and Moscow Ring Road are indicated in brown. Aerosol Complex MSU shown on the right.

2. Materials and methods

2.1. Study area

Moscow metropolitan area (55° 45′ N; 37° 37′ E at the city center; mean altitude 150 m a.sl.) is located in the center of the European part of Russia (map in Fig. 1). Moscow covers an area of 2561 km^2 and has a registered population exceeding 12.5 million within city borders, which makes it largest (interior only to Istanbul) and one of the most densely populated megacities in Europe. Fast urban expansion into new areas, intensive developing of transport feet, extensive construction of residential building and road infrastructure is a characteristic feature of a city since 1997 (Bityukova and Mozgunov, 2019). Largely populated (8.5 million people) and industry-developed area called as Moscovskaya Oblast takes place around the Moscow city (Fig. 1), thus the Moscow agglomeration is the biggest metropolitan area in Russia as well as in Europe. Spatial distribution of PM emissions for the region of Moscow agglomeration is presented in Fig.S1.

Moscow is the northernmost between the largest European cities; it is characterized by a humid continental climate (Dfb according Köppen climate classification). According to a record of the Meteorological Observatory MSU over the 60-year period (Chubarova et al., 2014), the significant warming of regional climate with a positive temperature trend of 0.07 °C/year is observed. It is influenced by the geographical position in the center of the East European Plain at the junction of the Smolensk-Moscow Upland in the west, the Moskvoretsko-Okskaya Plain in the southeast and the Meshcherskaya Lowland in the east and southeast, allowing cold and warm air mass to freely spread. Absence of peculiar orographic characteristics which can enhance the air mass stagnation creates conditions for the good pollution dispersion most of the year, except for cases of temperature inversions that can provoke the short-term accumulation of pollutants in the surface air layer (Lokoshchenko et al., 2021). Moderate average air temperatures, low solar UV radiation levels, and good ventilation make the accumulation of primary emitted pollutants and the photochemical formation of secondary pollutants less intensive in Moscow (Elansky et al., 2018). Icy winters with long-lasting snow deposits require an intensive road management in Moscow to prevent the traffic inconveniences.

Moscow city has a developed transport, heat and power production, and industrial infrastructure that use mostly fossil fuels (gas, diesel, gasoline, heavy oil). Gas consumption is dominated by heating supply and industry whereas motor vehicles use the most amounts of gasoline and diesel (Table S1). Fuel consumption in Moscovskaya Oblast differs by the higher usage of coal and less amount of heavy oil. Dense network of roads, high automobile fleet of around 7 million units (90.4 % passenger cars, 8.5 % trucks, 1.1 % buses) contributes traffic emission (SI). It composes up to 93 % of the overall emissions (Bityukova and Mozgunov, 2019). While automobilization is growing in Moscow, intensive implementation of higher ecological classes of engines, and better quality of fuel promote the improvement of vehicle ecological parameters. Standards below Euro-5 have been banned since January 2016. Over past 7 years, the large-scale road construction, development of public transport, improvement of the structure of vehicle fleet led to a density of emissions does not exceed 500 tons/sq.km/year for 70 % of the territory of a city (Bityukova and Mozgunov, 2019). Moreover, the restriction on the entry of heavy-duty (12 tons) trucks between the Moscow Ring Road and the Third Ring Road was introduced since January 2019, only at night time. Finally, the aerosol optical thickness (AOT) was decreased over last decade, its distribution over the Moscow megacity territory almost relates to highways and construction sites (Zhdanova et al., 2020).

Of industrial emissions, 50–65 % relates to combined heat and power plants (CHP), producing and redistributing energy and water; 20–30 % is emitted by refineries and 15–20 % by manufacturing industries (Bityukova and Saulskaya, 2017). A remaining 2–3 % of industrial emissions originate from the machinery and equipment industry, incinerators, food production and construction. CHP and residential sector in a city are almost totally supplied with natural gas (96.7 % of fuel consumption). Characteristics of thermal power supply are presented in SI.

Moreover, emission sources in Moscow as a northern megacity have several specific features. Centralized heating supply is seasonally operated from the end of September until the beginning of May. Combined thermal and power plants are almost totally use natural gas. Biomass is not used in a megacity either for industrial, domestic heating, or individual purposes, differently from many European and Asian cities (Amato et al., 2015; Diapouli et al., 2017a; Zhang et al., 2013). However, aerosol light absorption measurements indicted the biomass burning as a source of air pollution at the Moscow urban background, produced by residential heating/agricultural practice and transported by air masses from the area surrounding a megacity (Popovicheva et al., 2022). The snow melt and remobilization of salt applied to roads for deicing in winter impact on aerosol composition, thus revealing deicing as the particular source in Moscow similar to inland megacities (Zappi et al., 2023).

Assuming that currently the vehicles are powered with desulphurized fuels, traffic is no longer a significant source of SO_2 in Moscow. NO_2 constitutes a large fraction of gaseous pollution, its concentration is comparable while of sulfur dioxide, ozone, and carbon monoxide is much lower than in the large cities of industrialized countries (Elansky et al., 2007). The reason for that is the dominant using of natural gas as a fuel by the heating supply system, leading mainly to emissions of NO_x and CO from CHP (Elansky, 2014). Spatial distribution of SO_2 and NO_2 emissions for the region of the Moscow agglomeration is presented in Fig. S1.

The modern feature of the Moscow megacity is fast developing construction. In the period 2011–2019 around 5 million m^2 of the total area of the housing stock was built annually (SI). Every year, at least 100 km of roads are under construction, including engineering structures with tunnels, interchanges, bridges, overpasses.

2.2. Sampling site and campaigns

The measurement campaign was conducted at the Aerosol Complex MSU located at Meteorological Observatory of Moscow State University (MO MSU), southwest of the Moscow city (Fig. 1). MO MSU is not directly affected by local pollution sources such as large transport roads or industrial facilities. The residential area and a highway takes place about 800 m south of the observatory, industrial areas situate at a distance of 3 km and greater. Therefore, MO MSU site is classified as an urban background (Chubarova et al., 2014). MO MSU site is surrounded by nonpaved open ground area of MSU campus that may enhance the aerosol composition by soil and mineral dust contributions.

Within a radius of 15 km from MO MSU, there are about 150 stationary industrial sources of emissions; types of enterprises are indicated in Fig. 1 (see SI). In the territorial structure of indicated enterprises there are three main clusters. The western and southwestern cluster is represented by the Ochakovo industrial zone specializing on the food industry and building materials production, with CHPs and several boilers. The northern cluster is a result of deindustrialization and renovation of industrial zones, it has acquired a service specialization with enterprises for the disposal of various types of waste and the construction industry. The eastern and southeastern cluster is the most industrial area, mechanical engineering, machine-building; food and household chemical enterprises as well as a large CHP, numerous boilers and a waste incineration plant take places in this area.

An aerosol sampling system is installed at the pavilion of the Aerosol Complex MSU. Inlet supplied by an impactor takes place proximately 4 m above the ground. It supports the sampling with air flow of 1 $m^3\,h^{-1}$, the pumped volume is reported in standard atmospheric conditions. Particles with a diameter less than or equal to 10 μm (PM10) are daily collected over 24-h periods from 5 p.m. of a given day to 5 p.m. of the

next day. Quartz fiber filters of 47 mm (Pall Science, New York, USA), previously heated at 600 °C for 5 h, and polyethylene terephthalate 47 mm filters (Merck, Germany) were used for the following analyses by methods of analytic chemistry. PM10 mass concentrations were obtained using the TEOM 1400a (Thermo Environmental Instruments Inc., USA) by Mosecomonitoring.

PM10 sampling was performed during spring 2018 (from April 23rd to May 22nd), autumn 2019 (from September 5th to November 30th), and winter 2019–2020 (December 1st - January 18th). 31, 51 and 51 aerosol samples were collected in spring, autumn, and winter, respectively, totally 133 samples. Long vacation periods of New Year (from January 1st to 1^0th) and May (from 1st to 10th) public holidays were included. We should note the distinct characteristics of vacation times, namely during these days the economic and traffic activity of the Moscow population seriously drops. Moreover, because the beginning of the warm season during May holidays the significant part of population migrates from a city to the area surrounding city to their country houses. In winter, a majority of Moscow citizens lives inside the city because the continuous operation of the heating system.

2.3. Meteorological observations

Meteorological parameters (temperature, relative humidity, pressure, precipitation, wind speed, and wind direction) were measured at a 3 h time resolution by the MO MSU meteorological service. Time series of temperature, pressure, relative humidity, and precipitation during the whole study period are presented in Fig.S1. Table S2 shows the seasonal statistics of meteorological variables. Autumn 2019 and winter 2019–2020 with low mean temperature 5.4 ± 5.6 °C and 0.4 ± 2.1 °C, respectively, relate to the cold period. They were 2.3° and 6.1° above the average for 30 years of previous observations (Popovicheva et al., 2022).

Spring 2018 was characterized by significant changes in the air temperature, mass advection, and solar radiation (Chubarova et al., 2019). Mean spring temperature was 14.2 ± 4.8 °C and maximum exceeded 20 °C during May holidays. We note that fire activity is traditionally high in spring in the Moscow region when temperature rises; intensive agriculture fires in the regions around Moscow were recorded in spring 2018 (Popovicheva et al., 2022). Southwestern wind with the averaged speed of 1.4–1.5 m/s prevailed during all seasons, with highest wind speeds in autumn and winter.

Operation of centralized heating system begins and ends in Moscow when the temperature decreases below 8 °C and increases above 8 °C, respectively, thus separating the whole year on cold and warm periods. In 2018, the heating operation ended on May 6, so the spring sampling took place in both cold and warm periods. Autumn and winter sampling hold during the heating system operation, which began on September 23, 2019.

2.4. Analytic methods

For the elemental analysis of spring-time PM_{10} samples, the high energy, polarization geometry energy dispersive XRF spectrometer Epsilon 5 by PANalytical was used. Epsilon 5 is constructed with optimized Cartesian-triaxial geometry composing of several secondary targets for attaining lower spectral background. The used spectrometer is equipped with eight secondary targets (that can polarize the X-ray tube generated incident radiation through the Barkla scattering, see elsewhere (Manousakas et al., 2020). 21 elements determined by the ED-XRF method were Na, Mg, Al, Si, S, Cl, K, Ca, Ti, V, Cr, Mn, Fe, Ni, Cu, Zn, Br, Sr, Sb, Ba and Pb. The expanded uncertainty (including both analytical and sampling uncertainties) varied between 9 % (for S and K) and 38 % (for Sb). V was found below the detection limit for all samples. The detection limits varied between 0.48 and 17 ng/m^3, the lowest values were obtained for Cr, V, and Cl.

Summer and winter - time samples were analyzed by inductively coupled plasma mass spectrometry (ICP-MS) and atomic emission spectroscopy (ICP-AES), using the "X − 7c" mass spectrometer (Thermo Elemental, USA) and "iCAP-6500" atomic emission spectrometer (Thermo Scientific, USA), respectively. Concentrations of elements including major elements Al, Fe, K, Mg, Mn, Ti, Ca, S, and Na, and trace elements Ba, Bi, Cd, Co, Cr, Cs, Cu, Li, Mo, Ni, P, Pb, Sb, Sn, Sr, W, Zn, V, and As were determined after acid digestion (5 mL HF, 2.5 mL HNO3, 2.5 mL HClO4). A detailed description of the sample preparation procedure, a list of reagents used, and instrument settings are given in (Ivaneev et al., 2023). Analytic uncertainties were in the range of 15–30 % in dependence on element concentration. The detection limits varied between 0.3 and 30 ng/m^3 for major elements, and between 0.002 and 0.28 ng/m^3 for trace elements.

Thermo - Optical Transmittance method (TOT) is used for the determination of organic (OC) and elemental carbon (EC), using a Lab OC-EC Aerosol Analyzer (Model 5 L, Sunset Laboratory Inc., USA) and the EUSAAR2 protocol. Quartz filter samples were heated up to 650 °C in He, at first, and then up to 850 °C in a mixture of 2 % O_2 in He, using the controlled heating ramps of the EUSAAR_2 thermal protocol. OC evolved in the inert atmosphere, while elemental carbon EC was oxidized in the He—O_2 atmosphere. Charring correction was applied by monitoring the sample transmittance throughout the heating process, see elsewhere (Popovicheva et al., 2019a). The limit of detection (LOD) for the TOT analysis is 0.02 μg/m^3 of carbon. Lab and field blanks were prepared and run following the same procedures. The expanded uncertainty was calculated equal to 15 % for OC and 23 % for EC.

Water-soluble inorganic ion measurements were performed and described in (Zappi et al., 2023). Shortly, aerosol samples were analyzed for ionic species, namely cations, including Na^+, NH_4^+, K^+, Mg^{2+} and Ca^{2+}, and anions including Cl^-, NO_3^-, and SO_4^{2-}, using ion chromatography. Sample filters were placed into ultrapure water, shaken and filtered. Anions of spring samples were separated by an ion-exchange column (Ion Pac AS17A, Thermo Fisher, USA) in isocratic conditions using 1.8 mM Na_2CO_3 + 1.7 mM $NaHCO_3$. Cations were separated on Ion Pac CS12A using 38 mM methane sulfonic acid (MSA). In autumn samples, inorganic cations were determined using a Dionex ICS-1000 equipped with a gradient pump (ICS-3000 Model SP-1). Inorganic anions were analyzed using a Dionex ICS-5000+ IC., the guard column and analytical column were Dionex IonPac™ AG11-HC and Dionex IonPac™ AS11-HC, respectively. The detection limits varied between 2 and 20 ng/m^3, the lowest values were obtained for sodium and chloride. The expanded uncertainty varied between 16 and 20 %. We note that mineral potassium is less soluble than emitted by biomass burning; in our experimental data for K^+ represents the soluble potassium source.

2.5. Data analysis methods

2.5.1. Mass reconstruction

We reconstruct the aerosol mass on a seasonal basis by considering organic matter (OM), elemental carbon (EC), geological minerals, sodium chloride salt (NaCl), inorganic ions including SO_4^{-2}, NO_3^-, and NH_4^+ and trace elements such as V, Cr, Co, Ni, Cu, Zn, As, Sr, Cd, Sn, Sb, Cs, Ba, W, Bi, and Pb. OM is calculated by multiplying OC by a factor accounting for non-C atoms;, we adopted an empirical factor of 1.8 considering the urban background character of our site (Amato et al., 2015). Mineral dust [MIN] are assumed as the sum of major elements namely Al, Si, Ca, Ti, Fe, Mg, K, Mn, and soil-related Na (soilNa), all multiplied by factors to convert them to their common oxides (Al_2O_3, SiO_2, CaO, TiO_2, Fe_2O_3, MgO, K_2O, MnO, Na_2O) according to (Andrews et al., 2000) and (In't

Veld et al., 2021):

$$[MIN] = 2.14\cdot Si + 1.89\cdot Al + 1.43\cdot Fe + 1.67\cdot Ti + 1.4\cdot Ca + 1.20\cdot K + 1.66\cdot Mg + 1.29\cdot Mn + 1.35\cdot soilNa \quad (1)$$

Elemental Si was not analyzed by the ICP method used for autumn and winter samples, it was estimated using the (Si/Al) ratio derived from Si and Al concentrations; in our study Si concentration was estimated based on the abundance of Al and the Si/Al ratio of 3.821 in the upper continental crust (Rudnick et al., 2003). For spring time the Si/Al ratio were measured equal 3.6.

Given that Moscow is a typical inland city where sea spray - generated sea salt particles are not readily transported we should consider the other sources for chloride salt. The composition of de-icing agents used in the Moscow megacity is dominated by sodium chloride salts (see SI for details), thus the NaCl contribution corresponds to technical salt for road management. For mass reconstruction, NaCl mass was calculated assuming that water soluble Cl^- in aerosol samples is solely found in the form of NaCl (Diapouli et al., 2017a). Then, soil-related Na (soilNa) is calculated based on the crustal ratio Na/Al (0.298) and total NaCl mass is the sum of Cl^- and Na minus the soilNa mass.

One of the commonly used tool to differentiate OC from primary and secondary sources is presented in (Pio et al., 2011). Method for the evaluation of secondary organic carbon (SOC) in atmospheric particles is based on the minimum values for OC/EC ratio:

$$SOC = OC - (OC/EC)_{min}\cdot EC, \quad (2)$$

where $(OC/EC)_{min}$ ratio are estimated through a visual inspection of OC versus EC scatter charts, by drawing a best fit line through the origin and including points aligned in the lower edge of the chart (Pio et al., 2011).

2.5.2. Source apportionment by PMF

Source apportionment is performed by means of positive matrix factorization (PMF) model (Thunis et al., 2020). PMF produces two matrices (F -factor profiles and G - factor contributions) under the constraint of non-negativity for matrix F and non-significant negativity for matrix G. The model is based on the following mass balance equation:

$$c_{ij} = \sum_{k=1}^{p} g_{ik} \bullet f_{kj} + e_{ij} \quad (3)$$

where c_{ij} is the concentration of the chemical element j measured in the sample i, p is the number of factors (sources) that contributes to the measured concentrations, g_{ik} is the contribution of source k to the sample i, f_{kj} is the concentration of the chemical element j in the source k, and e_{ij} is the residual (the difference between the measured value and the value fitted by the model) for the chemical element j in the sample i.

The model solves the Eq. (3) by minimizing the sum of squared residuals for goodness-of-fit parameter Q:

$$Q = \sum_{i=1}^{n}\sum_{j=1}^{m}\left(\frac{c_{ij} - \sum_{k=1}^{p} g_{ik} \bullet f_{kj}}{u_{ij}}\right)^2 = \sum_{i=1}^{n}\sum_{j=1}^{m}\left(\frac{e_{ij}}{u_{ij}}\right)^2, \quad (4)$$

where u_{ij} is the uncertainty of the concentration c_{ij}. The Q value calculated through all data points is referred as "Q(true)". If points with large scaled residuals (usually >4) are excluded, the corresponding Q-value is referred to "Q(robust)"; thus the difference between Q(true) and Q (robust) is a measure of the impact of data points with high scaled residuals (Norris et al., 2014). Methodology of the best solution is described in the SI.

The chemical composition database of the PM_{10} samples (N=129) was used for the application of the EPA PMF 5.0 model. The species used in PMF analysis included all ions (Na^+, $NH4^+$, K^+, Mg^{+2}, Cl^-, NO^{3-} and SO_4^{2-}), except Ca^{2+} because the elemental Ca concentrations were used. Total S was excluded to avoid the double counting given its high correlation with SO_4^{2-}. Also, EC and OC as well as major and trace elements measured by both XRF and ICP (Al, Ca, Ti, V, Cr, Mn, Fe, Ni, Cu, Zn, Sr, Sb, Ba and Pb) were taken into account, excluding species already included as ions such as Na, Mg, S, Cl, and K. The database also includes five species measured only by ICP namely Cd, Sn, Mo, W and Bi because they are important tracers for anthropogenic emission sources. For these species, the values during spring were considered as missing ones and replaced by the median value of the remaining period. The final input database included 28 chemical species (OC, EC, Na^+, NH_4^+, K^+, Mg^{2+}, Cl^-, NO_3^-, SO_4^{2-}, Al, Ca, Ti, V, Cr, Mn, Fe, Ni, Cu, Zn, Sr, Cd, Sn, Sb, Ba, Pb, Mo, W and Bi) and PM_{10} as total variable.

2.5.3. Geographical origin of pollution sources

Method based on the bivariate polar plot (Carslaw and Beevers, 2013) shows how the concentration of species varies jointly with wind speed and wind direction in polar coordinates. This approach allows to trace the source location, preferably at scale ~1–10 km where the wind direction is remaining quasi-constant while the calculations of air mass transportation provides a limited support thanks to the low spatial resolution of the model employed. The highest values of concentrations identify the directions of emission source.

Backward trajectories (BWT) were generated using NOAA HYbrid Single-Particle Lagrangian Integrated Trajectory (HYSPLIT) model of the Air Resources Laboratory (Stein et al., 2015), with coordinate resolution equal to 1° × 1° of latitude and longitude. The potential source areas were investigated using 72 h back for air masses arriving at 500 m height above sea level (A.S.L.). The hourly final archive data were generated from the National Center for Environmental Prediction's Global Data Assimilation System (GDAS) wind field reanalysis.

Cluster analysis of trajectory data is an effective method of grouping the origin-like trajectories by combining the geographically data, it takes into account the features of seasonal atmospheric circulation (Zhang et al., 2013). The angular method is selected in which the matrix of angular distances shows how similar are two points of the BWT in dependence on their angle with respect to the initial location (Cui et al., 2021). Mean trajectory representing each cluster is calculated by grouping the BWTs with similar geographic origins using the angle - distance matrix. It is based on similarity of two back trajectory points depending on their angle from the starting location of the BWT. Fire information was obtained from Resource Management System (FIRMS), database MODIS (https://firms.modaps.eosdis.nasa.gov/map), operated by the NASA/GSFC Earth Science Data Information System (ESDIS).

3. Results and discussion

3.1. PM chemical composition

3.1.1. PM10 mass concentrations

Averaged daily data on PM_{10} mass concentrations for the whole study period are shown in Fig. 2. PM10 rarely exceeded the EU daily air quality guideline 50 μg/m^3 and Russian accepted limit 60 μg/m^3. Exceedance days for PM_{10} are presented in Table S2. PM_{10} demonstrated the minimal concentration at the averaged level 8.5 μg/m^3 during the New Year holiday due to the general decrease in traffic and population economical activities. The variation of PM_{10} versus the main meteorological variables during the whole study period reveals higher values detected in association with times of low or no precipitation, and low wind predominant from the southwest (Zappi et al., 2023). No significant correlation was observed between PM_{10} and temperature.

Table 1 and S3 provide a statistical summary of the obtained PM_{10} data. For the whole period the average PM_{10} was 22 ± 18 μg/m^3, with the seasonal value approached the maximum 33 ± 29 μg/m^3 in spring, and decreased to the minimum 14 ± 6 μg/m^3 in winter. We note that in spring 2017 and 2018, PM_{10} concentrations showed the similar relatively high PM_{10} levels (Popovicheva et al., 2020a). Thus, during the cold heating period the average PM_{10} concentration is found less than in

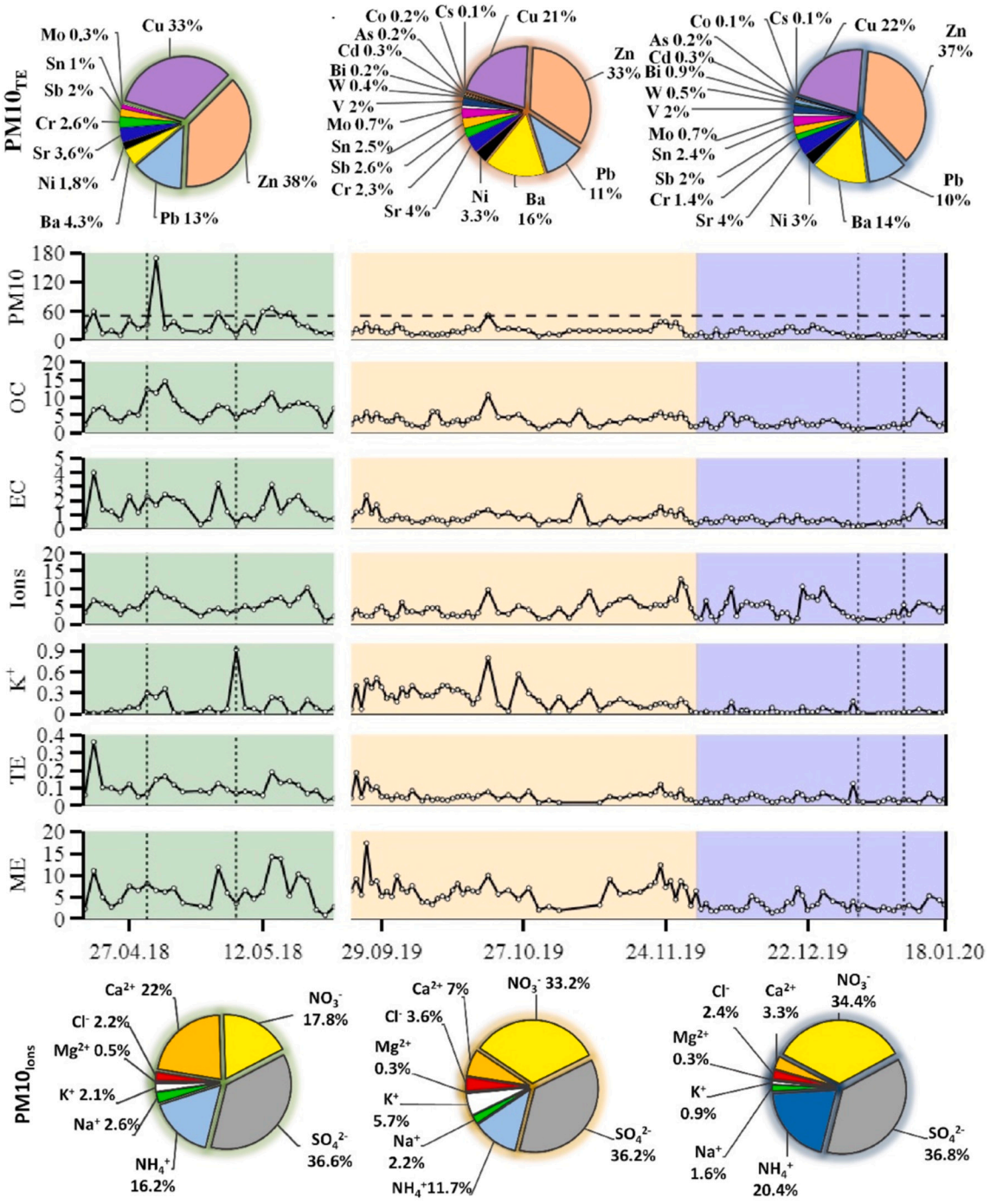

Fig. 2. Seasonal 24 h variations of PM10, OC, EC, and K^+ mass concentrations as well as total concentration of ions (Ions), trace elements (TE), and major elements (ME), in μg/m^3, in spring 2018 (green), autumn 2019 (yellow), and winter (2020–2021) (violet). Dash lines show EU daily limit. Percentage contribution of trace elements (top) and ions (bottom) to their overall content in $PM10_{TE}$ and $PM10_{ions}$, respectively, is shown. New Year and May holidays are indicated by dotted lines.

spring time. Increased spring particulate mass concentrations were observed in previous years and associated to soil re-suspension after the snow cover melted before vegetation activity (Gubanova et al., 2018).

Urban background PM_{10} annual mean values are smaller in north-western (London, 30 μg/m^3; Manchester, 32 μg/m^3) and central (Praha, 30 μg/m^3; Wien, 35 μg/m^3) and higher in southern Europe (Barselona 43 μg/m^3) (Putaud et al., 2010). High winter PM_{10} levels were recorded along a north-west to south-east European transect, ranging from 22 to 40 μg/m^3 (Alastuey et al., 2016). It should note that in winter, due to low thickness of the atmospheric boundary layer, numerical temperature inversions and stable stratification, the conditions for limited dispersion of airborne particulates and increased PM_{10} level are generally observed. Specific source given by residential wood burning during the cold period well relates to this feature; thus at urban background of large French cities PM_{10} reached 40 μg/m^3 in winter and falls to 10 μg/m^3 in the warm period (Favez et al., 2021). In Norwegian cities, particular in Oslo similar to central Europe, wood burning makes the largest contribution in winter (Yttri et al., 2011), despite the central heating system because the population prefer using the private facilities. Observations of markedly enhanced particulate mass in winter season in Chinese cities also reflects the impacts of heating activities (Yang et al., 2022).

Table 1
Descriptive statistics of meteorological parameters, measured concentrations of PM10 and chemical components over the whole study period (spring 2018, autumn 2019, winter 2019–2020). Total concentrations of ions (Ions), major elements (ME), and trace elements (TE).

Variables		Mean	sd	Median	1stQ	3rdQ	Min	Max
°C	T	5,7	6,7	15	0,9	10	-7,0	21
m/s	Wind speed	2,1	0,7	1,69	1,6	2,5	0,5	5
hPa	Pressure	993	10	995	987	998	972	1026
%	RH	77,8	14,9	55,94	70,2	90,1	37,1	100
mm	Precipitation	0,7	1,1	1,02	0	0,8	0	7
μg/m^3	PM10	22	18	18	12	25	7	169
	OC	4	2	4	2	5	1	15
	EC	0,9	0,6	0,7	0,5	1,1	0,2	4
	Na^+	0,1	0,08	0,08	0,04	0,1	0,003	0,4
	NH_4^+	0,70	0,5	0,6	0,3	1	0,003	2
	K^+	0,14	0,16	0,07	0,02	0,2	0,01	0,9
	Mg^{2+}	0,02	0,02	0,01	0,01	0,02	0,001	0,1
	Ca^{2+}	0,46	0,5	0,2	0,1	0,6	0,03	2,6
	Cl^-	0,13	0,14	0,07	0,04	0,2	0,002	0,8
	NO_3^{2-}	1,27	0,9	1	0,6	1,7	0,1	5
	SO_4^{2-}	1,61	1,1	1,4	0,8	2,1	0,2	6
	Ions	4,4	2,5	4,3	2,3	5,5	0,8	12
	Si	1,0	0,63	0,9	0,5	1,3	0,05	3,8
	Al	0,3	0,17	0,2	0,1	0,3	0,01	0,99
	Fe	0,4	0,26	0,4	0,2	0,6	0,1	1,4
	Ti	0,02	0,02	0,0127	0,007	0,02	0,0001	0,2
	Ca	0,6	0,45	0,5	0,3	0,8	0,07	2,2
	K	0,1	0,11	0,1	0,06	0,2	0,02	0,7
	Mg	0,1	0,06	0,0	0,02	0,08	0,004	0,3
	Mn	0,01	0,01	0,0	0,005	0,01	0,001	0,03
	Na	0,3	0,17	0,3	0,2	0,4	0,009	1,13
	S	0,3	0,2	0,3	0,2	0,5	0,06	1,1
	ME	5,2	3,0	4,6	2,7	7	0,6	17
ng/m^3	V	0,8	0,8	0,6	0,6	1	0,3	7,0
	Cr	1,4	1,1	0,9	0,43	2	0,0	5,0
	Ni	1,6	1,5	0,9	0,547	2	0,0	8,1
	Cu	16	19	10	5,8	22	1	178
	Zn	22	16	18	11,2	29	3	83
	Sb	1,4	3,1	0,6	0,2	1	0,1	27,8
	Ba	6,5	9,4	3,9	2,4	7	1,2	76,5
	Pb	7,1	7,9	4,0	2,1	9	0,6	54,8
	Mo	0,3	0,3	0,3	0,18	0	0,0	2,3
	W	0,2	0,2	0,1	0,053	0	0,0	1,9
	Bi	0,2	0,8	0,1	0,07	0	0,0	9,5
	Cd	0,1	0,1	0,1	0,08	0	0,0	1,4
	As	0,1	0,1	0,1	0,1	0	0	1,5
	Co	0,09	0,08	0,1	0	0,1	0	0,5
	Sr	2,3	5,1	1	0,8	2	0,2	42,4
	Sn	1,1	0,7	1	0,8	1	0,1	5,1
	Cs	0,03	0,06	0,00	0,00	0,0	0,00	0,20
	TE	61	45	50	33	74	16	359

In Milan, PM_{10} approached high concentrations up to 50 ± 28 μg/m^3 in winter and autumn (Amato et al., 2015), thus exceeding the Moscow urban background in 3.5 times. The atmospheric stagnation features of the Po Valley favored the accumulation of intensive winter PM emissions. Also, in Sofia megacity and midsize city Bolognia, located in a semi closed valleys, urban background PM_{10} concentrations in winter and autumn were above 40 μg/m^3 and in spring below 30 μg/m^3 (Hristova et al., 2020; Tositti et al., 2014). In Athens, a megacity also suffering from poor air quality due to topography and climatic conditions, PM_{10} were characterized by a higher spring level, up to 28 ± 19 μg/m^3 due to the African dust impact (Amato et al., 2015). Multiple exceedances of the EU daily air quality guideline, especially in the polluted megacities of China and India, resulted in frequent heavy pollution episodes during winter (Cheng et al., 2016). PM_{10} is the main air pollutant exceeding the ambient standards in most of the major cities in India where mean urban background 139 ± 75 μg/m^3 was recorded, due to fuel combustion in vehicles and coal-fired power plants as well as biomass, waste and residual oil burning (Gupta et al., 2012).

3.1.2. *Carbonaceous, ionic, and elemental fractions*

Organic carbon (OC) is primarily emitted in the particulate phase or secondary formed from gas-to-particle conversion processes. Elemental carbon (EC) is a major tracer for fossil fuel combustion, namely urban emissions from road transport, industry and heating systems. Other EC sources such as biomass burning are relevant to residential areas and wildfire events. The chemical composition of airborne dust depends on the geological peculiarities geology of the source region (Knippertz and Stuut, 2014), generated by wind erosion and soil re-suspension. Sulfate and nitrate are mainly produced by combustion of sulfur containing fuels, transport, and energy production. They derives from gaseous SO_2 and NO_x due to the oxidation to H_2SO_4 and HNO_3, respectively, under the influence of photochemically-driven processes (Hewitt, 2001). Precursor for ammonium, NH_3 mainly originates from farming activities and catalyzed gasoline engines. Water-soluble ions (ammonium, sulfate, and nitrate) are known as Secondary Inorganic Aerosol (SIA) (Seinfeld and Pandis, 2016). Dust may contribute to calcium and magnesium, usually in the form of soluble carbonates. K+ ion can be originated both from soil (mineral potassium) and biomass burning. Average daily data on the seasonally varying concentrations of aerosol components are shown in Fig. 2. Seasonal variability for OC, EC and well as exceedance days for OC and K^+ are reported in the Table S2. Statistic data over the whole study period and seasons are presented in Table 1 and S3, respectively.

Over the whole study period, the average OC was 4.1 ± 2.5 μg/m^3

with the maximum 6.7 ± 3.0 μg/m^3 in spring, and minimum 2.7 ± 1.3 μg/m^3 in winter. Chemical composition analysis in urban background of largest metropolitan urban areas in Greece (Athens and Thessaloniki) showed the opposite trend of significant increase of OC concentrations, up to 9.3 ± 7.9 μg/m^3 and 14.1 ± 5.2 μg/m^3 during the cold period, respectively (Diapouli et al., 2017a). That is pointed towards residential heating and more particularly wood burning as a significant source for residential heating in these megacities. Similar trend because the same reason but with significantly higher winter OC level (34.7 ± 10.2 μg/m^3) was observed for urban site in Delhi (Sharma et al., 2014), which is 13 times higher than the Moscow level. Over the whole period the average EC was 0.9 ± 0.6 μg/m^3, with similar to OC seasonal variability showing the maximum 1.5 ± 0.9 μg/m^3 in spring, and minimum 0.6 ± 0.3 μg/m^3 in winter (Table 1 and S1).

High correlation between EC and black carbon (BC) measured for the same periods in (Popovicheva et al., 2022) (Fig.S3) allow us to extend the present 24 h observations for EC by high - time resolution BC measurements and conclude about traffic effects combined with the boundary layer height from diurnal BC trends which exhibit morning and evening peaks. The weekly cycle of BC characterizes the highest amount of traffic-related pollution on working days and the lowest one due to population migration from a city to their country houses for weekends (Popovicheva et al., 2022).

The OC/EC ratio is an essential tool to differentiate the fossil fuel combustion (e.g. oil natural gas, coal) and biomass burning sources. We provide the knowledge about the OC/EC ratio in traffic exhaust, during the residential wood burning and woodstove combustion, wildfires and peat burning in the SI.

Data sets from urban background sites covering a wide geographical area in Europe have shown spatially and temporally consistent minimum ratios (OC/EC$_{min}$) of around 1.1–1.4, strongly impacted by traffic (Pio et al., 2011). Lower values were observed in larger cities than in smaller towns due to a less contribution of regional transport than local emissions. OC/EC ratios were relatively high during 2004–2018 in Beijing, with an average value of 3.4, indicating that there was significant SOC forming in PM (Ma et al., 2022). Especially from 2007 to 2018, OC/EC increased from 1.8 to 7.3, meaning that SOC pollution in Beijing was aggravated.

At the Moscow urban background the OC/EC ratio was found within the range of 1.6–9.6 (Fig.S3), with the mean of 4.9. In spring, autumn, and winter, the mean OC/EC ratio of 5.4, 4.6, and 4.7 was recorded, respectively, indicating an influence of other primary sources except traffic, with a higher OC/EC ratio. Long-range plumes of agriculture fires could increase OC/EC in spring. Biomass burning for residential heating is an obvious candidate in autumn and winter while we point onto an area surrounding Moscow because the central heating-gas fueled system operates in a megacity during the cold period.

Fig. S3 shows OC and EC concentrations in the PM10 Moscow urban background samples. (OC/EC)$_{min}$ ratios are obtained 1.6, 2.4, and 2.5 for spring, autumn, and winter, respectively (Fig.S4). These values were confirmed by additional calculation of medians for lower 5 % ratio value samples that are found quite similar. Such high (OC/EC)$_{min}$ indicates that there is a constant input of organic carbon added to vehicle transport - emitted aerosols in the Moscow urban background, possibly of secondary origin because the site location at a reasonable distance from roads and any emission sources. As observed in (Plaza et al., 2011), OC/EC ratio can increase is morning and evening traffic rush hours due to secondary aerosol production by photochemical processes, oxidizing freshly emitted volatile OC, and condensation. Moreover, the regional contribution of aged aerosol with higher secondary organic carbon content may increases the (OC/EC)$_{min}$ in the Moscow urban background.

Total water-soluble ionic concentrations show the average 4.4 ± 2.4 μg/m^3 over the whole study period. Sulfate ion SO_4^{2-} concentrations ranks the highest among ions analyzed, with mean of 1.6 ± 1.1 μg/ m^3 followed by nitrate NO_3^- (1.3 ± 1.9 μg/m^3), ammonium NH_4^+ (0.7 ± 0.5 μg/m^3), Ca_2^+ (0.5 ± 0.5 μg/m^3), Cl^- (0.12 ± 0.14 μg/m^3), K^+ (0.14 ± 0.16 μg/m^3), Na^+ (0.9 ± 0.08 μg/m^3), and Mg^{2+} (0.02 ± 0.02 μg/m^3). Total ionic concentration approached maximum 5.0 ± 2.3 μg/m^3 in spring, and similar 4.4 ± 2.5 μg/m^3 in autumn and winter, respectively.

Despite Moscow has the largest population among European (Amsterdam, London, Paris, Berlin) and Canadian cities (Toronto), data for the study period for the Moscow urban background show the lowest content of SO_4^{2-} and NH_4^+, and comparable NO_3^- (Zappi et al., 2023). Moscow average sulfate concentrations are comparable with ones in regional background sites of EMEP network in last decade, < 2 μg/m^3 for southern and northern Europe in winter, 0.5–1.1 μg/m^3 for central and northern sites in warm period (Alastuey et al., 2016). Such finding well relates to a fact observed in previous studies that nitrogen oxides constitute a large fraction of gaseous atmospheric pollution in Moscow, and their concentration is comparable to most of largest cities in industrialized countries due to intensive transport emissions while the average concentrations of sulfur dioxide, ozone, and carbon monoxide is much lower than in the majority of world megacities (Elansky et al., 2007). The reason for that was the dominant using of natural gas as a fuel, leading mainly to emissions of NO_x and CO from heating plants (Elansky, 2014) as well as low photochemistry impact of SIA formation (as will be discussed below).

Seasonal average SO_4^{2-} is 1.2 ± 1.1 μg/m^3 in spring, and almost similar 1.5 ± 1.3 μg/m^3 in autumn and winter. NO_3^- seasonal trend shows average concentrations less (0.8 ± 0.5 μg/m^3) in spring and higher (1.4 ± 1.0 μg/m^3) in autumn and winter.

SO_4^{2-} and NO_3^- were markedly enhanced from 3.5 and 11.0 μg/m^3 in the pre-heating to 13.1 and 23.2 μg/m^3 in the heating season due to the increased usage of coal/natural gas in the cold period in Chinese cities (Yang et al., 2022). Similar, residential heating commonly using wood leads to highest concentrations of SO_4^{2-} in winter in Central Europe (Stieger et al., 2018). Increased levels of sulfates in southern European cities, up to 3.0 μg/m^3 in Milan urban background, relates to the use of coal and petroleum coke/fuel oil for power generation as well as emissions of petrochemical plants (Amato et al., 2015).

However, the climate conditions in the southern cities change the trend of SO_4^{2-} and NO_3^- increase forward to the cold period. They pose the significantly higher temperature and solar radiation leading to sulfates in the warm period (5.2 ± 2.1 μg/m^3) are almost equal to the cold period (6.6 ± 3.9 μg/m^3) as a result of intensive photochemical processes of formation of secondary aerosols from urban and regional sources (Diapouli et al., 2017a). NO_3^- concentrations are found to be lower during the warm months, indicating loss of particulate nitrate to the gaseous phase due to high temperatures (Diapouli et al., 2017a).

K^+ seasonal average concentration varies from the highest 0.2 ± 0.1 μg/m^3 in autumn, 0.1 ± 0.1 μg/m^3 in spring to the minimum 0.02 ± 0.01 μg/m^3 in winter. Since K^+ is a commonly accepted marker of biomass burning (Gonçalves et al., 2010; Popovicheva et al., 2016), its maximum concentrations in spring 2018 and autumn 2019 confirms the impact from agriculture fires and residential heating in the area surrounding a megacity, as observed in (Popovicheva et al., 2022). Another reason for high K^+ in spring may be the biomass burning source consistent with higher springtime OC/EC mass ratio in spring (Fig.S3). A significant drop of K^+ in winter well relates to the decrease of the residential heating activity due population migration from the Moscow region to a megacity when the temperature drops significantly. Such seasonal concentration trend for K^+ shows the difference from cities where higher K^+ is observed during the winter months due to the increased using biomass for residential heating (Alastuey et al., 2016; Stieger et al., 2018).

Average Na^+ and Cl^- concentrations over the whole study period are comparable, 0.1 ± 0.08 μg/m^3 and 0.13 ± 0.14 μg/m^3, respectively. Na^+ seasonal concentration slightly varies from 0.13 ± 0.07 μg/m^3 in spring, 0.09 ± 0.08 μg/m^3 in autumn to 0.07 ± 0.08 μg/m^3 in winter (Table S1). Seasonal dynamics for chloride occurs because it is a highly reactive mobile substance degassed by atmospheric processing while conservative sodium accumulates in soil and stabilizes by ion exchange

chemistry then re-circulates in the atmosphere due to soil re-suspension (Zappi et al., 2023).

In inland cities the source of particulate sodium and chloride during the cold period is de-icing agents (DIAs) (Kolesar et al., 2018). Similar in Moscow, salt components (Na^+ and Cl^-) are attributed to a high amount of de-icing agents (mixtures NaCl, $CaCl_2$, or marble chips, see SI) used in road management (Eremina et al., 2015; Zappi et al., 2023).

For twenty five locations across the United States used to investigate the ubiquity of road salt aerosols, sodium and chloride concentrations were an average of 3 times higher in winter, as compared to summer (Kolesar et al., 2018). Low snow cover occurred in wither 2019–2020 in Moscow, with the maximum of 11 cm only in January that can be reason for losing the similar trend.

Ions, preferably derived from geological minerals, such as Mg^{2+} and Ca^{2+}, waxed in spring and followed by significant decrease towards autumn and winter. Ca^{2+} shows the maximum contribution of 22 % to the total ionic concentrations in spring due to the increase of fugitive dust after snow melting. The large variability of Ca^{2+} between seasons is influenced by industrial and construction being the water-soluble component of Ca (see below about Ca).

Total concentrations of major elements (ME) namely Al, Si, Ca, Ti, Fe, Mg, K, and Mn show the average 5.2 ± 3.0 μg/m^3 over the whole study period. Their seasonal trend is characterized by the highest mean of 5.9 ± 3.5 and 6.5 ± 2.8 μg/m^3 in spring and autumn, respectively, due to the strong impact of soil re-suspension and wind blowing, and by smaller one of 3.1 ± 1.3 μg/m^3 in winter when the permanent snow cover soil in Moscow. Out of all major elements, Ca has recorded at the higher concentration of 0.6 ± 0.4 μg/m^3 followed by Fe (0.32 ± 0.25 μg/m^3), Na (0.30 ± 0.17 μg/m^3), Al (0.26 ± 0.16 μg/m^3), and K (0.13 ± 0.11 μg/m^3).

For Ca, the highest average of 1.1 ± 0.6 μg/m^3 is in spring and around 5 times less in autumn and winter. The similar seasonal trend is found for the Ca/Al ratio, 3.5, 2.0 and 1.9, respectively, in general, it well correlates to total ME related to mineral dust. Additionally, Ca can be emitted by several sources such as construction and cement industry. *Re*-suspended calcareous dust mixed with rich Ca cement plant emissions were found near the city of Tirana (Almeida et al., 2020). Using the Ca/Al ratio, it is possible to indicate emissions from cement plants and building dust impact when it varies between 4 and 6 (Kong et al., 2011); this ratio in the upper part of the continental crust is strongly less, 0.23 (Rudnick and Gao, 2014).

Total concentrations of trace elements (TE) namely V, Cr, Co, Ni, Cu, Zn, Sr, Cd, Sn, Sb, Mo, Ba and Pb show the average 61 ± 45 ng/m^3 over the whole study period. They exhibit the similar seasonal trend as total ME, with the maximum 99 ± 60 ng/m^3 in spring, and minimum 37 ± 21 ng/m^3 in winter.

Although emitted in large proportion by industrial sources, Cu is often a tracer of non-exhaust vehicle emissions (Amato et al., 2015). Levels of Sb and Sn are relatively higher at the transport-influenced as compared with urban background sites, due to non-exhaust vehicle emissions including brake and tyre wear (Gietl et al., 2010). Major portions of transition metals Ba, Fe, and Mn are released through abrasive vehicular emissions which is frequently occurring near traffic lights; the friction between brake pad and linings decomposes the wear of brake linings (Birmili et al., 2006). Zn may be contributed from galvanized materials, vehicle body and tire wear, it is useful in the rubber production. Zn and Ca may be also emitted from the combustion of lubricating oil (Viana et al., 2008). Ni is commonly associated with V and is used to trace combustion of fuel oil; however it is also emitted by metallurgical processes (iron and steel manufacturing). Sources of As, Pb, and Cd are related to high-temperature processes such as coal combustion, roasting and smelting of ores in non-ferrous metal smelters and melting operations in ferrous foundries (Alastuey et al., 2016).

Sr concentrations at Moscow urban background for study period are found near to those observed in Barcelona and Florence; Pb, Sb are comparable while Zn, Sn, Ba are less a few times while Zn, Pb, Sb, Sn, Ba far exceeds (up to one order of magnitude) the level of Moscow pollution (Amato et al., 2015). Seasonal concentrations less in Moscow than Athens are observed for Zn but in winter only for Pb they are less while in the warm period Sb and Ba are higher at the Athens urban background (Diapouli et al., 2017a). Concentrations of Ni and V are always higher in Athens indicating significant impact of heavy oil consumption, in shipping also. PM10 urban backgrounds of Turkish and Indian cities is strongly enriched with Ni, Cr, Mo (up two orders of magnitude) in comparison to Moscow (Bozkurt et al., 2018; Sharma et al., 2014) which is a distinguished signal of industrial activities and coal combustion.

Species commonly associated with primary emissions are EC, primary organic matter (POM), salt (NaCl), and mineral dust. During the atmospheric processing secondary inorganic aerosol (SIA) and organic matter (SOM) are formed from inorganic and organic gaseous precursors and may behave in different manners. The former preferentially forms in the hot and humid seasons via photochemical reactions, although their precursor gases, such as SO_2 and NO_x, are emitted much more in winter. The latter seems to favorably form in the cold and dry seasons. The amount of secondary aerosol is a sum of SOM and SIA.

Secondary OC (SOC) was estimated from measured OC and $(OC/EC)_{min}$ ratios for each season using Eq. (2). SOC contributes from 2.1 to 83.3 % to OC for the whole study period, with mean 49 %. Seasonal SOC variations are 43 % in winter, 44 % in autumn, and 67 % in spring. (Zhang et al., 2013) estimated that secondary OC represents more than half of the measured OC at Chinese regional sites (~ 67 %) and urban sites (~ 57 %).

Fig. 4 shows primary and secondary aerosol fractions of PM_{10} mass, SOM was estimated from SOC and multiplied by 1.8. For the calculation of the secondary and primary aerosol contributions, all values are normalized by the sum of reconstructed PM_{10} mass. For the whole study period, the primary aerosol contribution prevails, 62 %. It is similar to 63 % observed for the urban traffic site in Porto but different from urban backgrounds in southern European cities (Milan and Athens) where the organic and inorganic secondary contributions to PM10 are very well balanced (close to 50 %) (Amato et al., 2015). In winter, primary aerosol drops down 56 % while secondary approaches 44 %, thus the contribution of both become practically equal at Moscow urban background.

SIA contribution gradually increases from spring to winter, from 20 to 34 %, while SOA has the largest proportion (22 %) in spring and a minimal (10 %) in autumn and winter. Such SIA contribution increase from spring to winter indicates the influence of particular source of secondary inorganic species such as transport and centralized heating supply by CHP. Distinct characteristics of Moscow CHP emissions is the increase in the cold period because the low temperature. In European urban areas, SIA contribution grows to up to 28 % of PM_{10}, owing to the extensive use of combustion at all the scales from industry down to domestic and individual uses (Putaud et al., 2010; Tositti et al., 2014). A number of studies investigated the sources of SIA and SOA in China indicated that fossil fuel combustion and industrial emissions are the most important sources of SIA (contributing 63–88 % of SO_4^{2-}, and 47–70 % of NO_3^-), and agriculture emissions are the dominant source of NH_4^+ (contributing 54–90 %) (Zhu et al., 2018).

3.2. PM_{10} mass balance

The mass reconstruction analysis is performed to obtain the assessment of chemical aerosol composition by summing the relative abundance of the different species in the carbonaceous, ionic, and elemental fractions (Fadel et al., 2022). By employing the method in Section 2.5.1, we construct the mass closure of PM10 at the Moscow urban background. The proportions of various fractions in PM_{10} mass measured together with unaccounted constituents as a whole are schematically illustrated by pie charts (Fig. 3). Overall over the whole study period, the major components are OM, mineral dust, and sulfate which account for 34 %, 24 % and 7 % of PM_{10} mass, respectively. The minor components include EC (4 %), nitrate (6 %), ammonium (3 %), chloride salt (2 %),

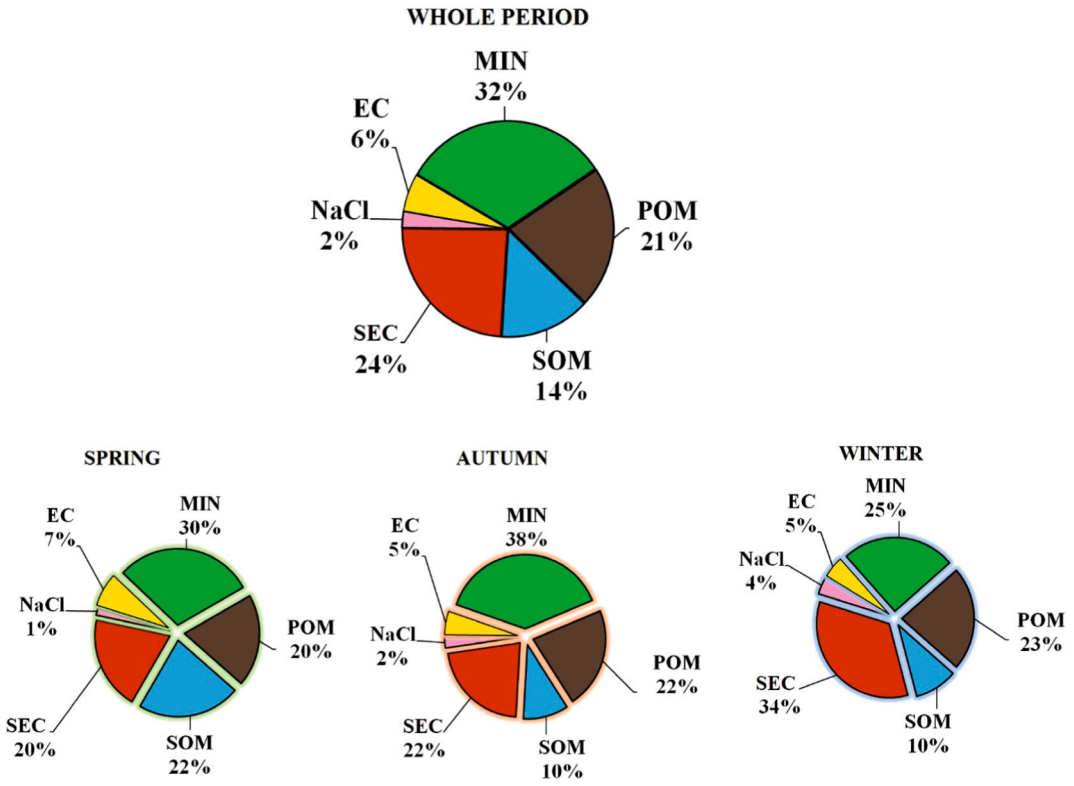

Fig. 3. Primary (POM, MIN, EC, NaCl) and secondary (SIA, SOM) aerosol fractions of PM10 mass during the whole study period, in spring 2018, autumn 2019, and winter 2019–2020.

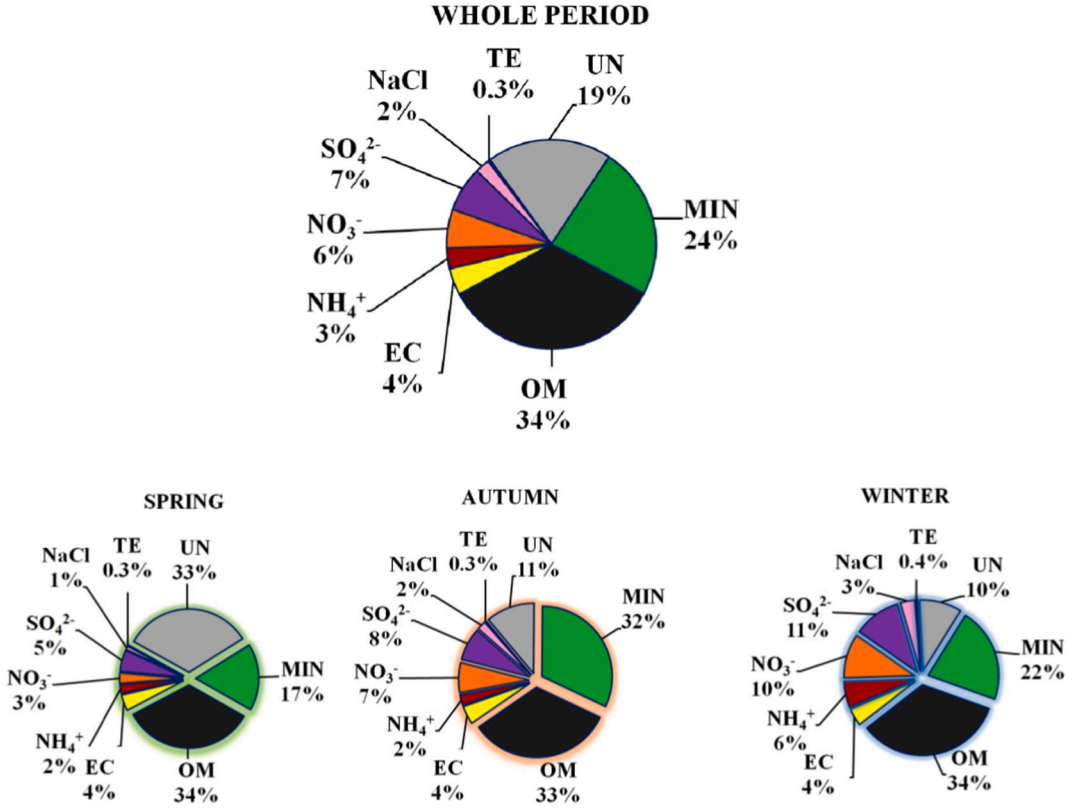

Fig. 4. Pie-charts showing the reconstructed chemical mass closures for PM10 during a whole study period, in spring 2018, autumn 2019, and winter 2019–2020. The components include mineral dust (MIN), organic matter (OM), element carbon (EC), sulfate, nitrate, ammonium, NaCl, and total concentration of trace elements (TE). Other than identified components is unaccounted fraction (UN).

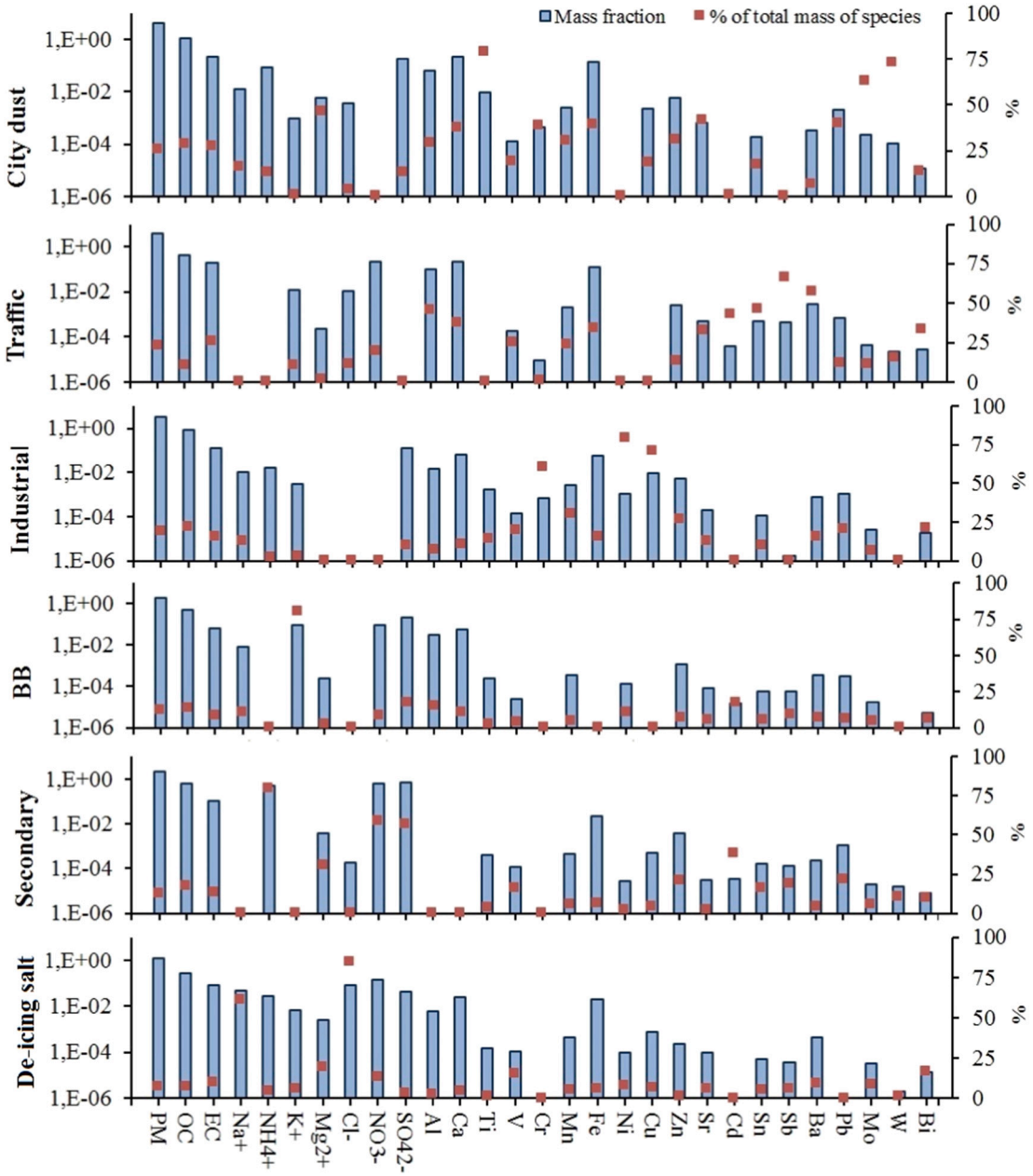

Fig. 5. PMF factor profiles of city dust, traffic, industrial, biomass burning (BB), secondary, and de-icing salt sources identified in PM10. The light blue bars (left axis) represent concentrations as mass fractions in μg/μg, red dots (right axis) represent the percentage of each chemical element's mass that is assigned to each source.

and trace elements (0.3 %). Totally SIA composes 16 % of PM_{10} mass.

OM accounts for around 34 % in PM_{10} mass in any season. It is different from that as observed in northwestern and southern European cities where OM contributions are higher in winter, pointing towards a significant impact from biomass-fueled residential heating (Diapouli et al., 2017a; Waked et al., 2014). EC contribution represents on average 4 % of PM10 mass in any season, together OM and EC accounts 38 %.

The second contributor to PM_{10} mass is mineral dust, with the increase of its fraction from spring (17 %) to autumn (32 %), and then the decrease in winter (22 %). Increases in mineral dust levels in southern and central Europe is typically observed during the warm season when dry conditions favor the soil dust re-suspension as well as due to Saharan dust outbreaks, ranging on average between 10 and 29 % (Alastuey et al., 2016; Diapouli et al., 2017b). High levels of mineral dust at eastern European sites were attributed to local or regional sources.

SO_4^{2-} and NO_3^- contributions show the seasonal increase from 5 % and 3 % in spring to 11 % and 10 % in winter, respectively well correlating with the temperature decreasing and heating period. NH_4^+ impact is less but showing the same trend of increasing from 2 % in spring to 6 % in winter. For the total contribution of SIA we obtain the maximum 27 % in winter, exceeding mineral dust, and 17 % in autumn and just 10 % in spring. The opposite higher contribution of SIA in the warm period, 42 %, and 27 % in the cold one was observed in southern megacities relating to the increased photochemical gas-to-particle conversion processes (Diapouli et al., 2017a). SIA dropped three times from spring to winter at the Istanbul urban background (Koçak et al., 2011). On average, there is more OM contribution to PM_{10} at urban background sites in central and northwestern Europe and more sulfate and nitrate in southern Europe while the highest contribution of mineral dust is related to impact of Sahara dust in southern Europe (Putaud et al., 2010). Unaccounted (UN) constituent is obtained by subtracting the sum of estimated aerosol fractions mass from PM10 measured mass (Fig. 3). One

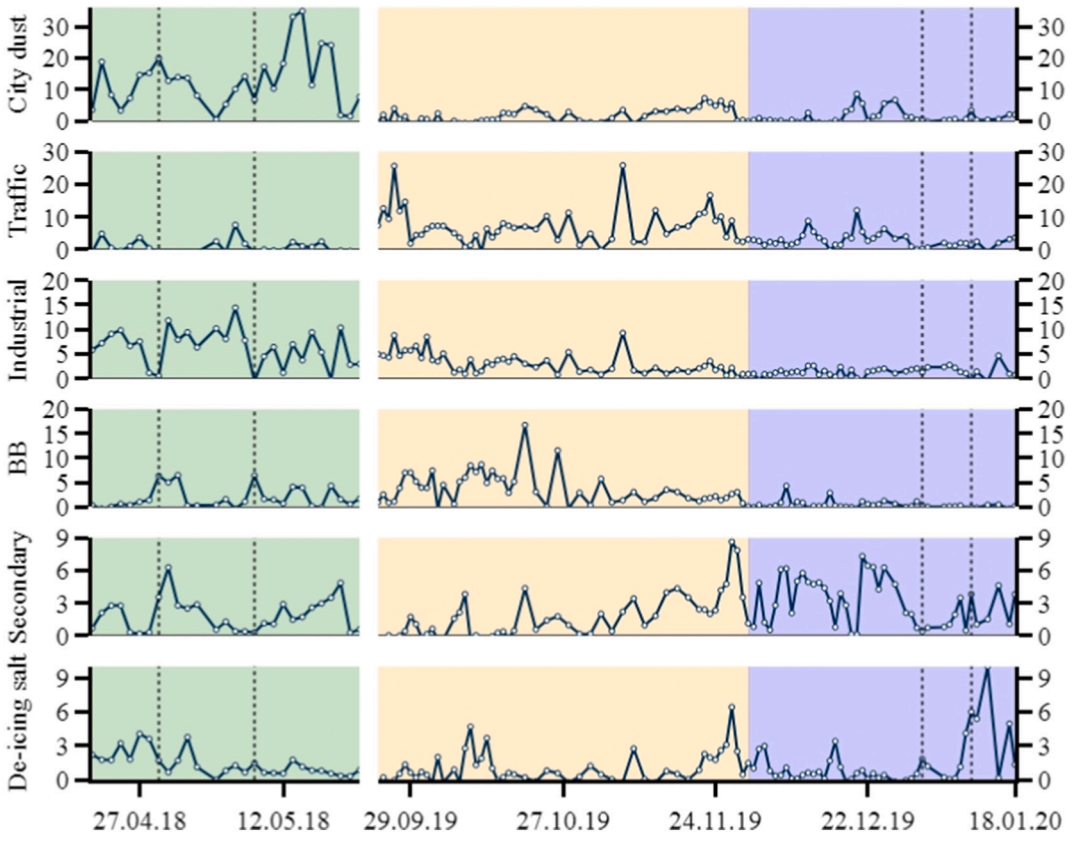

Fig. 6. Temporal variation of daily PMF factor contributions (in μg/m^3) during the whole study period. New Year and May holidays are indicated by dotted lines.

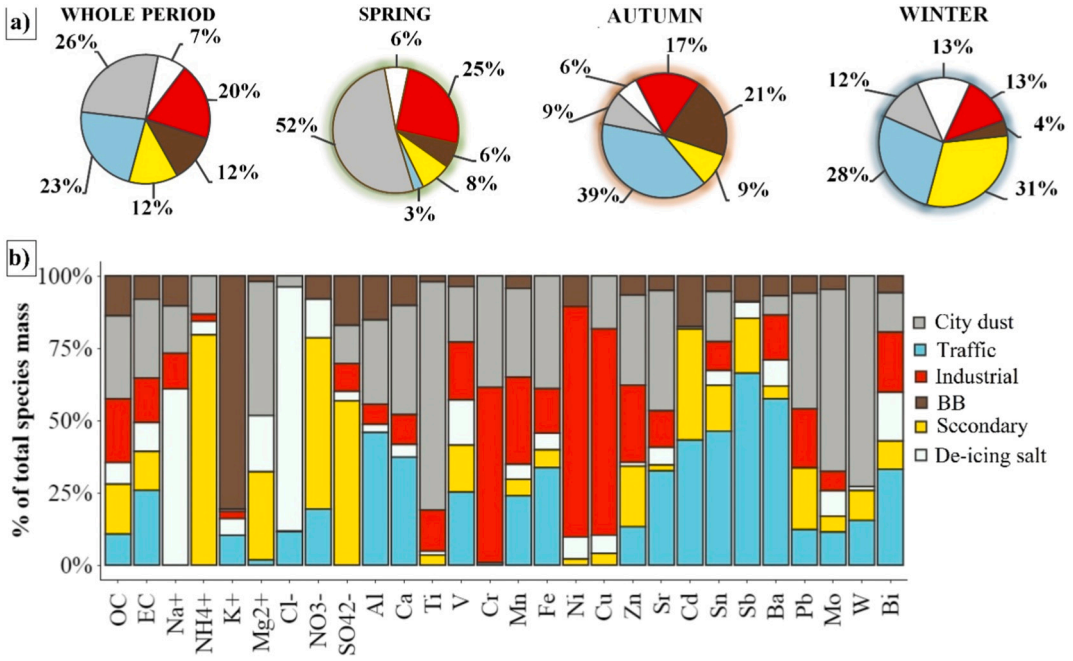

Fig. 7. a) Average relative source contributions to PM10 for the whole period of study, for spring 2018, autumn 2019, and winter 2019–2020: values are presented as percentage of PM10. b) Relative mass of aerosol components (%) apportioned to each factor/source.

observes that the reconstructed mass has allowed getting results relatively close to the measured PM_{10} mass, UU mass percentage represents on average 19 %.

During New Year holiday, in the period of strong decrease of traffic and economic activity, the mass balance shows the slight difference from the winter one: OM contribution increased up to 42 % whereas mineral dust decreased down to 16 %, also because the snow coverage at that time (Fig. S4). Contribution of sulfate and nitrate could not be changed because the city heating supply was uninterruptable.

3.3. Source identification and apportionment

Six main sources obtained for PM_{10} at the Moscow urban background are evaluated by the distinctive characteristics of each modeled source profile. City dust, traffic, industrial, secondary, biomass burning, and de-icing salt are presented by factor profiles (the relative mass contribution of each chemical species to PM mass, μg/μg) (Fig. 5). The time series of daily concentration contributions are illustrated for each source in Fig. 6. Average relative source contributions to PM_{10} for the whole period of study and relative mass of aerosol components apportioned to each factor/source are shown in Fig. 7.

The first factor is city dust: it has the largest contribution (26 %) in PM_{10} mass among all the factors. This factor accounts for a large fraction of the total mass of Ti (79 %), Al (29 %), Ca (38 %), Mg (46 %) and Fe (39 %); these elements are typically used as tracers for soil re-suspension (Alastuey et al., 2016). Ca content is higher than Al in the city dust profile (ratio is 3.5), that indicates Ca-rich dust. For comparison, the geochemical analyses of the topsoil horizons of landforms located in the uncontaminated area of the central part of European Russia (Kaluga region, around 200 from Moscow) shows Ca/Al = 0.13 (Samonova et al., 2020). Emphasizing that calcium is an indicator for construction dust with the high Ca/Al ratio >6 (Kong et al., 2011; Zhang et al., 2013) whereas for road dust and soil blowing it is 0.8–1.3 (Kong et al., 2011), we can conclude about potential construction impact on the Moscow city dust composition. High percentage of Sr (31 %) in this profile also proves the construction impact (Amato et al., 2015). Sulfates related to this factor can originate from salts such as $CaSO_4$ and $Al_2(SO_4)_3$ which are produced by cement plants, also relevant to the construction.

The city dust factor profile contains accounts for a large fraction of the total mass of Mo (62 %), W (72 %), Cr (40 %), Zn (31 %), Pb (39 %), and Cu (18 %). The presence of these species points towards resuspended city dust, including soil enriched with anthropogenic species emitted by the different activities (construction, traffic, large industrial plants and small-scale manufacturers). Comparison between the city dust profile obtained by PMF and a characteristic profile of the PM_{10} dust collected from roads in the city (Vlasov et al., 2021) shows good agreement (Fig. 8) that further supports the identification of this factor as city dust rather than soil dust. Chemical analysis of dust collected from roads in Moscow has indicated an OC content varying from 0.2 to 6.7 % (Kasimov et al., 2019). The relative contribution of OC in this factor (0.5 %) falls within this range. In the eastern part of the Moscow city, the accumulation of trace element Mo, Sb, Cd, Sn, Bi, Co, and As in road dust is the most pronounced while in the western part Pb, Cu, Cr, and W are prominent (Kasimov et al., 2020; Vlasov et al., 2023).

The second factor is traffic, identified by high EC and OC concentrations as well as the high percentage of the total mass of Sb, Sn, Cd, and Ba. It contributes 23 % to PM_{10} mass. Tail pipe emission relates to EC and OC (Watson et al., 2008); the ratio OC/EC equal to 2 for this factor can act as a good indicator of vehicle emission being closer to fresh - emitted traffic (Pio et al., 2011). Higher values of OC/EC between 2 and 3.7 links to the long distance from main roads (Amato et al., 2015). Sb, Sn, Cd, and Ba are trace elements for brake wear (Harrison et al., 2021); their mass high percentage of 66 %, 46 %, 43 %, and 57 %, respectively, indicate metal profiles of various non-exhaust vehicle emissions. We should note that Cu does not contribute any mass into Moscow traffic factor; but it contributes to the city dust profile.

The third factor is industrial pollution; it is characterized by high OC, EC, Mn, Zn, Ba, Pb concentrations and high percentage of total mass of Cr (60 %), Ni (79 %), and Cu (71 %). It contributes 20 % to PM_{10} mass. The high impact of Cr, Mn, Zn is attributed to industrial sources as metal manufacturing plants and storage (Sharma et al., 2014). Presence of Zn, Pb, S, Cu, Cd, Sb and Mn indicates high - temperature metal processing (Amato et al., 2015). The ferrous/nonferrous metallurgical pollution are identified by a mixture of several traces such as Mn, Fe, Pb, Zn, Cu, and Cr (Almeida et al., 2020). Examination of species in the Moscow industry factor and metal manufacturing industry profiles in European database SPECIEUROPE (Pernigotti et al., 2016) shows some similarities. V contributes by a small mass fraction, only 10 %, and the ratio V/Ni (equal to 0.1) is significantly lower than typical V/Ni ratios reported for heavy oil combustion (2–3) (Becagli et al., 2012) showing the limited impact of heavy fuel usage in Moscow industrial facilities. The industry factor accounts for 10 % of total Ca mass, while the Ca/Al ratio in the profile is equal to 4.1, that is high enough to suggest the possible construction and cement plants impact into this source.

The forth factor relates to biomass burning (BB) because of high (80 %) of K^+ mass is assigned to this source. It contributes 12 % to PM_{10} mass. Ratio OC/EC in this factor is equal to 8.3, being well in the range of typical BB and aged emissions (Diapouli et al., 2014). Photo-oxidation of BB emissions during transport enables production of significant amounts of secondary organic aerosol. The BB source for the Moscow urban background is associated with air mass transportation from largely populated region Moscovskaya Oblast which applies wood burning for domestic heating of country houses, garden cleaning work, and weekend and holiday recreational activities. Agriculture fires may be a reason for higher OC/EC ratio observed in spring, as demonstrated by the seasonal variability of the BB profile.

The fifth factor is relevant to secondary inorganic and organic aerosol, it dominates by high concentrations of SO_4^{2-}, NO_3^-, and NH_4^+ which relative mass contribution apportioned to this source is 55, 59, and 79 %, respectively. It contributes 12 % to PM_{10} mass. This factor is the result of secondary aerosol formation in the atmosphere. SIA components may be formed by local gaseous precursors and/or may be linked to long-range transport of anthropogenic emissions from the Moscow region or further away. Formation of NH_4^+ is facilitated by

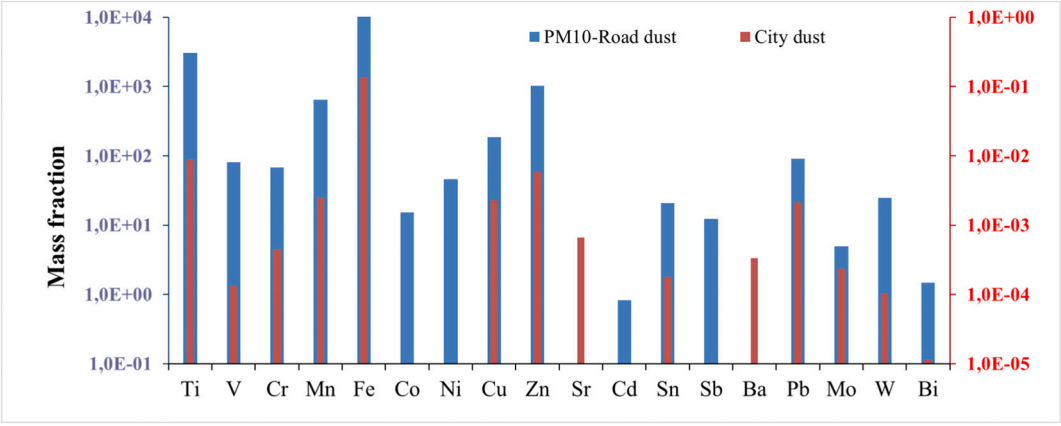

Fig. 8. Profiles of city dust factor and potentially toxic elements in PM10 road dust (Vlasov et al., 2021).

urban garbage dumps, wastewater, and transport from agricultural areas of the Moscow region. OC and EC also contribute around 15 % of relative mass in this factor with high OC/EC ratio equal 6.2 which confirms the secondary character of this factor. Finally, the sixth factor named as de-icing salt accounts for most of the mass of Na^+ (60 %) and Cl^- (84 %), followed by Mg^{2+} (19 %) and NO_3^- (13 %).It contributes 7 % to PM_{10} mass. The factor profile indicates the presence of sodium chloride salt, most likely from de-icing agents. De-icing salt is widely used to prevent the icing of the Moscow roads. Secondary nitrate is present probably in the form of nitrate salts $NaNO_3$ and is the result of local NOx emissions reacting with salt aerosol.

Comparison for the temporal variation of modeled city dust source with the observed seasonality of major elements (Fig. 2) shows that the maximal and minimal contributions of mineral dust in spring and winter, respectively. It is consistent with the similar seasonality of the city dust factor relating to intensive soil/dust re-suspension in spring (with contribution to PM_{10} of 52 %) and to the snow coverage which decreases the city dust factor contribution down to 12 % in winter. This consistency indirectly verifies the reliability of PMF results.

For traffic factor, the time series do not reveal evident seasonality, except clear decreasing during May and New Year holidays because low public transport and economic activity. Temporal variation of BB factor contribution indicates the maximum in autumn (21 %) due to dominant impact of residential BB, well in correlation with observations of dominant aerosol light absorption (Popovicheva et al., 2022). Significant decrease in winter down to 4 % relates to the peculiarity of the Moscow region population migration in the cold period when almost all citizens live in a city. Averaged secondary source contribution to PM_{10} strongly increases from 8 % in spring and 9 % in autumn to 31 % in winter. The reason for that is the intensive sulfate and nitrate emission from CHP in the cold period when the seasonal variability shown in the secondary source is driven by nitrate, which is favored by low

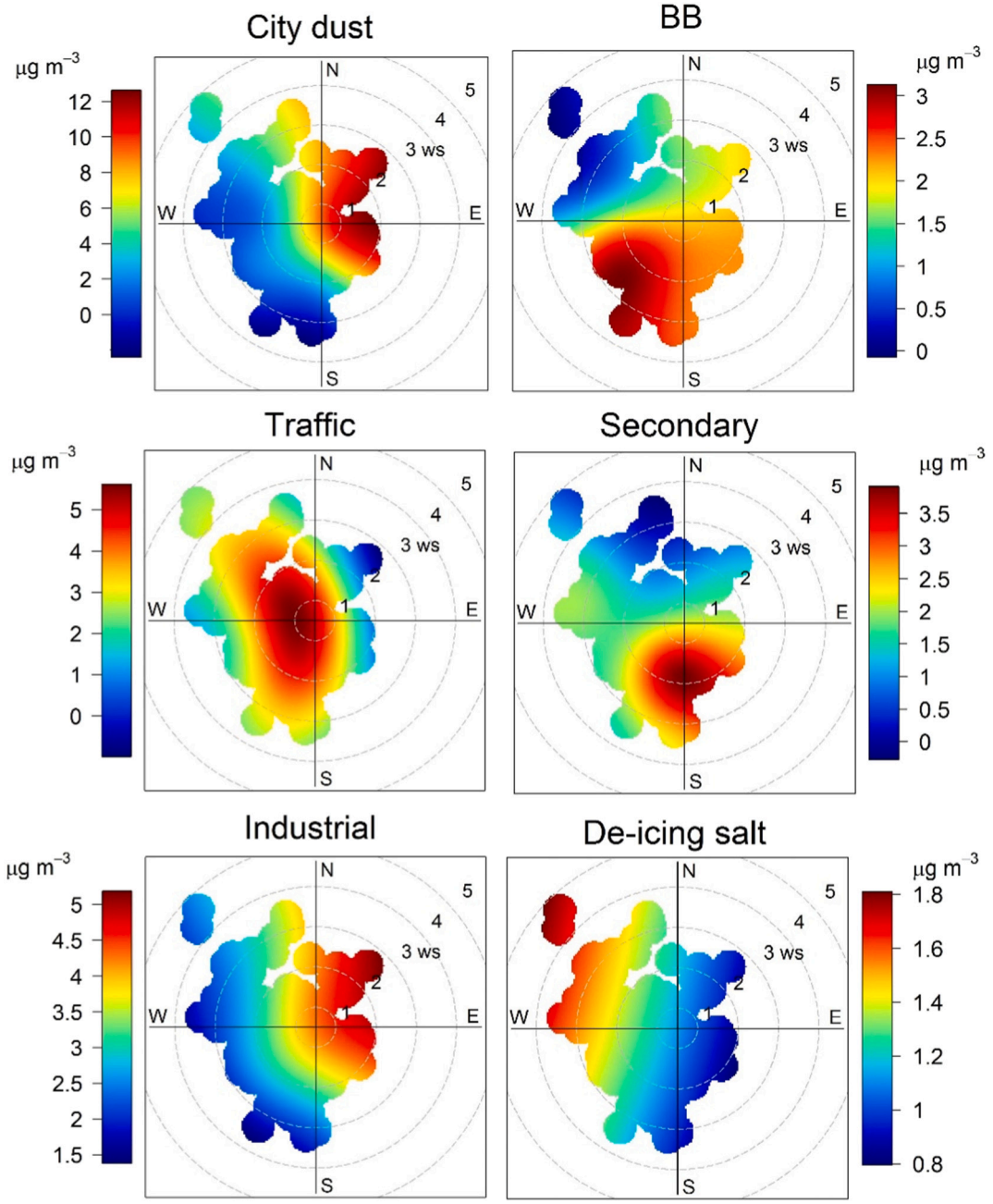

Fig. 9. Factor polar plots as a function of wind direction (°) and speed (ms^{-1}) during the whole study period.

temperatures and high humidity. Whereas low temperature and solar radiation in Moscow even in warm seasons does not support intensive photochemical processes of formation of SIA. This is also apparent in the seasonal variability of SO_4^{2-} and NO_3^-: no seasonality in SO_4^{2-} and winter highs in NO_3^-. The temporal variation of modeled de-icing salt profile indicates the intensive use of salt in winter, purposely in January when snow cover becomes stable. At that time the contribution of this factor to PM10 reaches 13 % and decreases down to 6 % in other season.

Individual source contributions are estimated for days of exceedance of the PM_{10} European daily guideline value (50 μg/m^3) (Table S3).

3.4. Anemological source origin analysis

Meteorological factors contribute significantly to variability of aerosol components; wind direction analyses is often complement to receptor model solutions (Watson et al., 2008). Traffic, biomass burning, fuel oil combustion, and sea salt sources reveals a clear relationship to the wind direction from polar plots (Saraga et al., 2021). The wind rose for the whole study period shows the prevailed wind direction from northwest to south with speed between 0.5 and 2.5 m/s (Fig.S6), in accordance to the long-term observation of southwest wind direction for the MO MSU (Chubarova et al., 2014). Fig. S7 shows the bivariate concentration polar plots for PM_{10}, OC, EC, selected ionic, and elemental concentrations for the whole study period, providing a graphical representation of the their source origin. We should note that there is a significant diversity in the direction of aerosol component origin which does not necessary coincides with the prevailing wind.

Polar plots for PMF factors are presented in Fig. 9. City dust factor demonstrates the polar plot similar to PM_{10} mass concentration, being its larger contributor. It reveals the source origin in the northern and northeastern directions where the Moscow city center with the most intensive road traffic and the northern industry cluster with waste disposal, utilities, and construction enterprises take place (map Fig. 1). OC polar plot well coincides with the city dust as the biggest fraction of PM_{10}. Additional source for city dust is located in the southeast, pointing on the largest plant producing cement and asphalt. The same source direction is identified from polar plot for Ca as a marker of cement production.

Traffic factor tends to be associated with weak winds when non-buoyant ground level sources are important. Very identical polar plot with uniformly spatially distributed source is obtained for EC as the major marker of traffic. Increasing wind speed generally results in lower concentrations due to dispersion and mechanical turbulence. Secondary factor polar plot indicates the pollution sources in the south and southeast where the most industrially developed cluster with large CHPs, boilers and a waste incineration plant take place (map Fig. 1). Polar plots of SO_4^{2-} and NH_4^+ show a very similar pattern indicating the same origin for ammonium sulfates in the southeast (Zappi et al., 2023). High concentrations of NO_3^- in the south well reflect the secondary factor origin. According the spatial distribution of SO_2 and NO_2 emissions, the highest emitters are located in the Moscow region (Fig.S1).

The industry sources contribute from multiple directions. A higher component originates from the eastern and southeastern industrial cluster with numerous enterprises of mechanical engineering, machine - building, food and chemical production (map Fig. 1). High percentage of industrial source contribution is observed in spring when the northeastern direction is associated with prevailed wind. We note the large similarity between industry and city dust polar plots that indicate almost the same directions for sources of both factors.

Regarding the BB source, the highest contribution corresponds to southwest that pinpoints the Ochakovo industrial zone and residential areas in New Moscow. The latter is supported by the similar polar plots for the marker BB source component K^+ in autumn (Zappi et al., 2023), in the period of the highest impact of biomass burning (Popovicheva et al., 2022). De-icing source is influenced mainly by northwestern winds; its polar plot is a result of superposition of both for Cl^- (source is enhanced under almost all observed wind directions) and Na^+ (source corresponding to the direction of the main roads near MO MSU site).

3.5. Source regions deduced from trajectory cluster analyses

Source region analyses allow the addressing of the air mass origin and estimating the relative importance of emitters in different regions (Molnár et al., 2017). Frequencies of air mass transportations by 72 h BWT cluster analysis are shown for spring 2018, autumn 2019, and winter 2019–2020 in Fig. 10. Four clusters are separated from western (W), northern (N), northwestern (NW), southeastern (SE), and southern (S) directions. Mean concentrations of PM10 and main aerosol components in identified trajectory clusters together with estimated percentages of each cluster in a total are presented in Table S4 and Fig. S8. Estimation of source regions impact is based on daily BB, secondary, city dust, and industry factor contributions (Table S4); traffic and de-icing is assumed to be preferably local source because denser road network is concentrated in the Moscow city. For all seasons, the W cluster is characterized by the biggest amount of BWT but the highest mean concentrations of aerosol species and contributions of various factors seasonally vary with air mass clustering and not always correspond to the prevailing W cluster.

In spring 2018, the highest concentration of PM10 (36 ± 24 μg/m^3) is associated with the W cluster which includes 36 % of BWT. The highest BB factor (1.9 ± 3.0 μg/m^3) in this cluster indicates that the BB source impacts the air pollution of a megacity from the western direction,. Such finding relates to large agriculture fires occurred in the European part of Russia and around Moscow in spring 2018 (Popovicheva et al., 2022; Popovicheva et al., 2020a). Additionally, the residential sector in Moscovskaya Oblact could impact with using of biomass for house heating and cleaning the gardens. In spring 2018, the secondary factor (4.0 ± 1.5 μg/m^3) relates to the NW cluster (29 %) and contributes with a maximum (4.0 ± 1.5 μg/m^3) between others in this cluster. BWT at that time passed over northwestern regions of Moscow agglomeration where the largest industrial emitters of SO_2 and NO_2 take place (Fig. S1 and description in SI). City dust factor has the similar highest contribution around 15 μg/m^3 in N (29 %) and NW (18 %) clusters. North of Moscow agglomeration where the largest plants and manufacturers take place is associated with the highest PM emissions (Fig. S1). Industry factor shows a small difference between clusters, in average 6.45 ± 0.7 μg/m^3, the dominant industrial source region for springtime.

In autumn 2019, the highest BB factor (5.1 ± 4.1 μg/m^3) is associated with prevailed air mass transportation from the W cluster (46 %). Wildfires occurred during 72 h of their transportation are shown in Fig. 11. The secondary (4.2 ± 2.1 μg/m^3) and industry (3.8 ± 2.1 μg/m^3) factors contributes a maximum in the SE cluster (19 %). At this time north and northwest of Moscow agglomeration are associated with the highest PM emissions where the largest plants and manufacturers take place (Fig. S1). The same SE direction (18 %) dominates the highest city dust contribution (4.1 ± 9.5 μg/m^3) but three times less that in spring. However, the SE cluster did support the highest industry contribution, different from other clusters which are almost equal, in average 3.2 ± 0.5 μg/m^3.

In winter 2019–2020, the W cluster includes a big amount of BWT (56 %) whereas the highest concentrations of PM_{10} are associated with the S cluster (11 %). BB factor contributes significantly 0.5 ± 0.9 and 0.9 ± 0.1 μg/m^3 in S and SE (13 %) directions, respectively. The largest industrial emitters in south of Moscow agglomerations are presented in Fig. S1. BWTs from almost all directions, SE(13 %), S(11 %), NW(20 %), define the city dust factor, in average 1.6 ± 0.1 μg/m^3.

3.6. Comparison of Moscow source apportionment with large cities

Typical for urban background factors/sources were obtained for many European and Asian cities. In (Belis et al., 2013) six major source

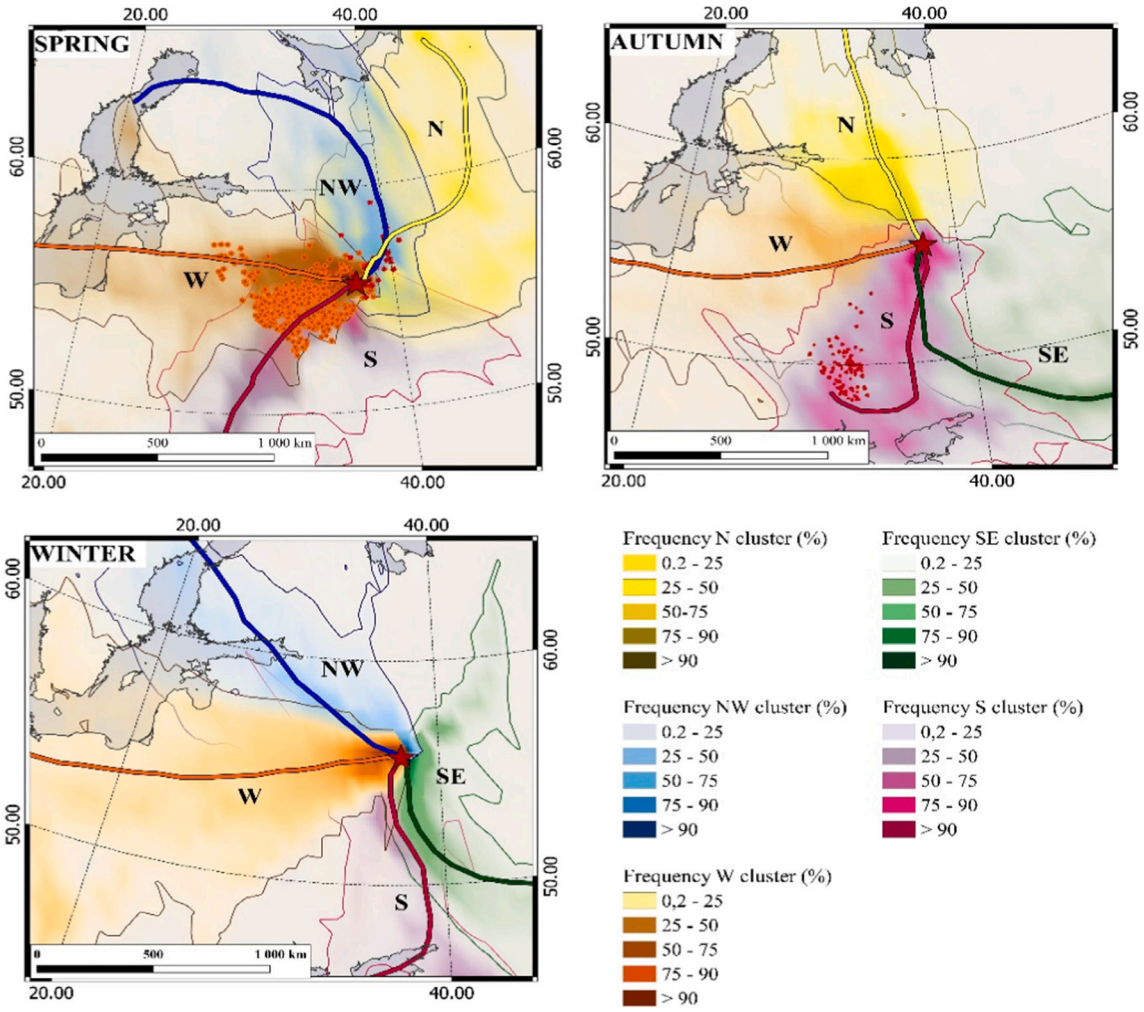

Fig. 10. 72 h BWT frequencies for spring 2018, autumn 2019, and winter 2019–2020 shown with color scale. Thin lines of the same color limit the areas with a frequency >5 %. Major directions of air mass transportations by BWT cluster analysis defied as NW, N, W, S, and SE. Main trajectories representing each cluster shown by the same color. Fires related to BWT which arrive at exceedance days (May 9, 2018 and October 20, 2019) indicated by red sports. Star is MO MSU site.

categories for PM_{10}, namely secondary aerosol, traffic, re-suspension of mineral dust, biomass burning, industrial, and sea/road salt were apportioned in Europe. The factor of fossil fuel (FF) combustion was associated with the petrochemical industry, residual oil combustion, and coke production in the most industrialized areas recognized as a European hotspot for air pollution (Masiol et al., 2020; Padoan et al., 2020) while the major influence of secondary processes are underlined for regional background site (Waked et al., 2014). Studies throughout Europe agreed on the identification of main sources in PM10: vehicular, crustal, sea-salt, mixed industrial/fuel-oil combustion, and secondary aerosol (Viana et al., 2008). Mineral dust source is characterized by elements abundant in the earth's crust and soils. The proximity of southern Europe to large dust emitting areas is responsible for the frequent transport of Sahara dust over southern Europe. On annual average for 52 European urban sites, dust source contribution to PM10 mass is 24 ± 11 % that is the second after secondary aerosol (Belis et al., 2013). This result is consistent with the evaluation for Moscow city dust contribution, on average of 26 % for the study period when it found a dominant source. For comparison, dust, fossil fuel combustion, transportation, biomass burning, industrial emission, secondary inorganic and secondary organic aerosol are the main source categories of fine PM identified in China (Zhu et al., 2018).

Secondary source is the aerosol formation in the atmosphere due the photochemical oxidation of sulfur and nitrate oxides and volatile organic, combined with ammonium. At European urban sites the relative contribution from secondary source to PM_{10} is 30 ± 6 %. Because high radiation and low wet deposition, its contribution is significantly higher in urban background of southern cities where it approaches up to 32 % in the warm period (Diapouli et al., 2017a). Moreover, the secondary factor could be separated on two for southern cities: secondary sulfate & organics and secondary nitrate & organics (Amato et al., 2015; Diapouli et al., 2017a). That is opposite to Moscow urban background where the maximum contribution of secondary aerosol 31 % is observed in the cold period. Nitrate drives the seasonal trend towards winter due to more intensive operation of centralized heating supply in the cold period. Higher impact of SIA and SOA in cold period is also typical for Chinese cities where fossil fuel combustion and industrial emissions are the most important sources (Zhu et al., 2018).

Source categories that encompass emissions deriving from many different vehicle types and associated processes were incorporated into the traffic (Belis et al., 2013). It is evaluated as the third most intense source for PM_{10} in Europe: at urban sites the relative contribution from traffic to PM_{10} is 23 ± 9 %. Main traffic source could be separated on two: vehicle exhaust and vehicle non-exhaust (Amato et al., 2015; Diapouli et al., 2017a). Non-exhaust emissions have become an increasing proportion of the total emissions, in many countries can exceed exhaust emissions (Harrison et al., 2021). For the Moscow urban background, the traffic factor cannot be separated while the road dust markers are appeared in both traffic and city dust, probably due to a high contribution of mineral dust highly mixed with road dust in

multiple emission - loaded urban atmosphere. The peculiarity of Moscow traffic is its high seasonal variability, approaching 39 % in autumn, it relates to distinct season population activity and climate conditions.

Large variability among cities concerning BB is mostly due to the different degree of using biomass in the residential heating. Contribution of BB source in many southern European cities is relatively high, 15–20 %, in winter. A district *heating system* is used as centrally located boilers or water *heaters* that circulate heat energy to individual customers. Except in Barcelona (Spain) where 96 % of homes are heated by natural gas (Amato et al., 2015; Diapouli et al., 2017a). BB source has been reported to be one of the major sources in Asian cities, particularly in winter due to combustion of wood (Sharma et al., 2014). In the Moscow city natural gas is using for residential heating by centralized heating supply, however the BB factor composes as much as 21 % in autumn and decreases down minimum, 4 %, in winter. The reason for that is the long-range transportation of residential BB from the Moscow region which impact relates to season -dependent activity of the population in areas surrounding a city.

Industry factor is a rather heterogeneous category including emissions from oil combustion in power plants together with different types of industrial (petrochemical, metallurgic, construction, ceramic, etc.). High levels of Ni and V indicates the heavy oil burn, therefore in cities where residual oil is intensively used in industry and shipping, the fuel oil combustion is identified as a standalone source like in Tirana, Banja Luka, Zagreb, Athens, Belgrade, Dushanbe, and Skopje (Almeida et al., 2020). It is different for Moscow where the fuel oil combustion is not identified as a separated factor probably due to limited heavy oil usage (Table S1).

Sea/Road salt includes profiles characterized by Na, Cl, and Mg that can be attributed either to sea salt in areas close to the coast or to road salt in continental areas of Central and Northern Europe (Belis et al., 2013). Salt - related source is also characteristics for Moscow as for the northern inland city with the abundant de-icing road management. Similar de-icing salt factor contributes PM10 in northern cities Oslo (Laupsa et al., 2007) and Augsburg (Gu et al., 2011), in Bologna where the "pseudo-marine" contribution presents higher levels during the cold periods (Tositti et al., 2014).

4. Conclusions

In Moscow, the largest and northernmost European megacity, the climate and dense population imposes the peculiar conditions onto economical activity, fuel consumption, heating system operation, and road management. Aerosol characterization and source apportionment firstly performed for the Moscow urban background during the cold heating period (autumn and winter) and warm springtime shows a number of the distinct characteristics. The absence of orographic features favors the megacity to be not under the significant impact of conditions which can contribute to the accumulation of pollutants. PM_{10} mass demonstrates rare cases of exceeding the European 24 h limit values. PM10 approaches the maximum in spring due to soil/dust resuspension after snow melted and minimum in winter, different from many European and Asian megacities. Residential BB and agriculture fires in the region around the Moscow city identified by increased K^+ marker. Impact the OC and EC is maximum in spring. High OC/EC ratio indicates the strong regional impact of aged aerosol and residential activity on carbonaceous aerosol. A significant drop of K^+ in winter relates to the decrease of the residential heating activity due the population migration to the city, in opposite to cities with higher BB impact because increased residential heating. Centralized heating supply fueled by natural gas leads to SO_4^{2-} concentrations more comparable to ones in European regional background sites than to cities where wood, petroleum coke/fuel oil is widely used for residential heating and power generation. Low temperature and solar radiation in Moscow does not support intensive photochemical processes of SIA formation; the SIA contribution to the mass balance has the maximum during the heating period. Primary and secondary aerosol fractions of PM_{10} mass are almost equally important in winter.

PMF model identifies six sources for PM_{10} at the Moscow urban background. City dust dominates following by traffic, different from many European cities with the most significant secondary aerosols. City dust includes re-suspended soil polluted by anthropogenic sources, including construction; last one is distinctly prominent because of the fast developing of the Moscow agglomeration in the last decade. Traffic encompasses emissions from exhaust and non-exhaust of vehicles mixed with mineral dust in the multiple emission-loaded urban atmosphere. Contribution of secondary aerosols driven by nitrate significantly increases from spring to winter showing the same trend as SIA in the mass reconstruction. BB contribution reveals a pronounced spring and autumn time, despite European and Asian cities where emissions from BB remain a major driver of winter aerosol pollution due to using of biomass for residential heating. Trace elements in the industrial factor indicate the impact of metal manufacturing plants. All of mentioned factors are influenced by long - range transport from western, northern, and southern populated and industrialized regions surrounding the city. De-icing is a major source of the ubiquity of road salt aerosols with no negligible impact in autumn and summer because the different mobility and remobilization of salts. PM_{10} concentrations that exceed the current European air quality limit indicate city dust and industrial factors as the most important sources to target for abatement together with regional biomass burning. This study quantifies the major emission sources of PM_{10} in Moscow urban background and thus provides the crucial information about air quality in largest and northernmost megacity, presenting a framework for tackling the aerosol pollution.

Funding

Authors thank to the Russian Science Foundation (project No. 19–77–30004–П) for a support of the PMF apportionment methodology developing. Aerosol characterization was performed under grant of the Ministry of Science and Higher Education of the Russian Federation (No. 075–15–2021–574).

CRediT authorship contribution statement

Olga Popovicheva: Writing – review & editing, Writing – original draft, Methodology, Investigation, Conceptualization. **Evangelia Diapouli:** Validation, Methodology, Data curation. **Marina Chichaeva:** Visualization, Validation, Software, Formal analysis, Data curation. **Natalia Kosheleva:** Funding acquisition. **Roman Kovach:** Validation, Formal analysis, Data curation. **Viktoria Bitukova:** Resources, Investigation. **Konstantinos Eleftheriadis:** Methodology, Conceptualization. **Nikolay Kasimov:** Supervision.

Declaration of competing interest

The authors declare that they have no known competing financial interests or personal relationships that could have appeared to influence the work reported in this paper.

Data availability

Data will be made available on request.

Acknowledgment

Research was carried out with equipment of MSU Shared Research Equipment Center "Technologies for obtaining new nanostructured materials and their complex study" and National Project "Science".

Appendix A. Supplementary data

Supplementary data to this article can be found online at https://doi.org/10.1016/j.scitotenv.2024.170315.

References

Alastuey, A., Querol, X., Aas, W., Lucarelli, F., Pérez, N., Moreno, T., et al., 2016. Geochemistry of PM 10 over Europe during the EMEP intensive measurement periods in summer 2012 and winter 2013. Atmos. Chem. Phys. 16, 6107–6129.

Almeida, S., Manousakas, M., Diapouli, E., Kertesz, Z., Samek, L., Hristova, E., et al., 2020. Ambient particulate matter source apportionment using receptor modelling in European and Central Asia urban areas. Environ. Pollut. 266, 115199.

Amato, F., Alastuey, A., Karanasiou, A., Lucarelli, F., Nava, S., Calzolai, G., et al., 2015. AIRUSE-LIFE+: a harmonized PM speciation and source apportionment in 5 Southern European cities. Atmospheric Chemistry & Physics Discussions 15.

Andrews, E., Saxena, P., Musarra, S., Hildemann, L., Koutrakis, P., McMurry, P., et al., 2000. Concentration and composition of atmospheric aerosols from the 1995 SEAVS experiment and a review of the closure between chemical and gravimetric measurements. J. Air Waste Manage. Assoc. 50, 648–664.

Baklanov, A., Molina, L.T., Gauss, M., 2020. Megacities, air quality and climate. Atmos. Environ. 126, 235–249.

Becagli, S., Sferlazzo, D., Pace, G., Di Sarra, A., Bommarito, C., Calzolai, G., et al., 2012. Evidence for heavy fuel oil combustion aerosols from chemical analyses at the island of Lampedusa: a possible large role of ships emissions in the Mediterranean. Atmos. Chem. Phys. 12, 3479–3492.

Belis, C., Karagulian, F., Larsen, B., Hopke, P., 2013. Critical review and meta-analysis of ambient particulate matter source apportionment using receptor models in Europe. Atmos. Environ. 69, 94–108.

Birmili, W., Allen, A.G., Bary, F., Harrison, R.M., 2006. Trace metal concentrations and water solubility in size-fractionated atmospheric particles and influence of road traffic. Environ. Sci. Technol. 40, 1144–1153.

Bityukova, V.R., Mozgunov, N.A., 2019. Spatial features transformation of emission from motor vehicles in Moscow. Geography, environment, sustainability 12, 57–73.

Bityukova, V., Saulskaya, T., 2017. Changes of the anthropogenic impact of Moscow industrial zones during the recent decades. Vestnik Moskovskogo Unviersiteta, Seriya Geografiya 3, 24–33.

Bozkurt, Z., O. Gaga, E., Taşpınar, F., Arı, A., Pekey, B., Pekey, H., et al., 2018. Atmospheric ambient trace element concentrations of PM10 at urban and sub-urban sites: source apportionment and health risk estimation. Environ. Monit. Assess. 190, 1–17.

Carslaw, D.C., Beevers, S.D., 2013. Characterising and understanding emission sources using bivariate polar plots and k-means clustering. Environ. Model Softw. 40, 325–329.

Cheng, Z., Luo, L., Wang, S., Wang, Y., Sharma, S., Shimadera, H., et al., 2016. Status and characteristics of ambient PM2.5 pollution in global megacities. Environ. Int. 89-90, 212–221.

Chubarova, N., Belikov, I., Gorbarenko, E., Eremina, I., Zhdanova, E.Y., Korneva, I., et al., 2014. Climatic and environmental characteristics of Moscow megalopolis according to the data of the Moscow State University Meteorological Observatory over 60 years. Russ. Meteorol. Hydrol. 39, 602–613.

Chubarova, N.E., Androsova, E.E., Kirsanov, A.A., Vogel, B., Vogel, H., Popovicheva, O. B., et al., 2019. Aerosol and its radiative effects during the Aeroradcity 2018 Moscow experiment. Geography, Environment, Sustainability 12, 114–131.

Cui, L., Song, X., Zhong, G., 2021. Comparative analysis of three methods for HYSPLIT atmospheric trajectories clustering. Atmosphere 12, 698.

Diapouli, E., Popovicheva, O., Kistler, M., Vratolis, S., Persiantseva, N., Timofeev, M., et al., 2014. Physicochemical characterization of aged biomass burning aerosol after long-range transport to Greece from large scale wildfires in Russia and surrounding regions, Summer 2010. Atmos. Environ. 96, 393–404.

Diapouli, E., Manousakas, M., Vratolis, S., Vasilatou, V., Maggos, T., Saraga, D., et al., 2017a. Evolution of air pollution source contributions over one decade, derived by PM10 and PM2. 5 source apportionment in two metropolitan urban areas in Greece. Atmos. Environ. 164, 416–430.

Diapouli, E., Manousakas, M.I., Vratolis, S., Vasilatou, V., Pateraki, S., Bairachtari, K.A., et al., 2017b. AIRUSE-LIFE+: estimation of natural source contributions to urban ambient air PM 10 and PM 2. 5 concentrations in southern Europe–implications to compliance with limit values. Atmos. Chem. Phys. 17, 3673–3685.

Elansky, N., Lokoshchenko, M., Belikov, I., Skorokhod, A., Shumskii, R., 2007. Variability of trace gases in the atmospheric surface layer from observations in the city of Moscow. Izvestiya. Atmospheric and Oceanic Physics 43, 219.

Elansky, N.F., Ponomarev, N.A., Verevkin, Y.M., 2018. Air quality and pollutant emissions in the Moscow megacity in 2005-2014. Atmos. Environ. 175, 54–64.

Eremina, I., Aloyan, A., Arutyunyan, V., Larin, I., Chubarova, N., Yermakov, A., 2015. Acidity and mineral composition of precipitation in Moscow: influence of deicing salts. Izvestiya, Atmospheric and Oceanic Physics 51, 624–632.

Fadel, M., Ledoux, F., Seigneur, M., Oikonomou, K., Sciare, J., Courcot, D., et al., 2022. Chemical profiles of PM2. 5 emitted from various anthropogenic sources of the Eastern Mediterranean: cooking, wood burning, and diesel generators. Environ. Res. 211, 113032.

Favez, O., Weber, S., Petit, J.-E., Alleman, L.Y., Albinet, A., Riffault, V., et al., 2021. Overview of the French operational network for in situ observation of PM chemical composition and sources in urban environments (CARA program). Atmosphere 12, 207.

Gietl, J.K., Lawrence, R., Thorpe, A.J., Harrison, R.M., 2010. Identification of brake wear particles and derivation of a quantitative tracer for brake dust at a major road. Atmos. Environ. 44, 141–146.

Ginoux, P., Prospero, J.M., Gill, T.E., Hsu, N.C., Zhao, M., 2012. Global-scale attribution of anthropogenic and natural dust sources and their emission rates based on MODIS Deep Blue aerosol products. Rev. Geophys. 50.

Golitsyn, G.S., Grechko, E.I., Wang, G., Wang, P., Dzhola, A.V., Emilenko, A.S., et al., 2015. Studying the pollution of Moscow and Beijing atmospheres with carbon monoxide and aerosol. Izvestiya Atmospheric and Oceanic Physics 51, 1–11.

Gonçalves, C., Alves, C., Evtyugina, M., Mirante, F., Pio, C., Caseiro, A., et al., 2010. Characterisation of PM10 emissions from woodstove combustion of common woods grown in Portugal. Atmos. Environ. 44, 4474–4480.

Gu, J., Pitz, M., Schnelle-Kreis, J., Diemer, J., Reller, A., Zimmermann, R., et al., 2011. Source apportionment of ambient particles: comparison of positive matrix factorization analysis applied to particle size distribution and chemical composition data. Atmos. Environ. 45, 1849–1857.

Gubanova, D., Belikov, I., Elansky, N., Skorokhod, A., Chubarova, N., 2018. Variations in PM 2.5 surface concentration in Moscow according to observations at MSU meteorological observatory. Atmospheric and Oceanic Optics 31, 290–299.

Gupta I, Salunkhe A, Kumar R. Source apportionment of PM10 by positive matrix factorization in urban area of Mumbai, India. Sci. World J. 2012; 2012.

Harrison, R.M., Allan, J., Carruthers, D., Heal, M.R., Lewis, A.C., Marner, B., et al., 2021. Non-exhaust vehicle emissions of particulate matter and VOC from road traffic: a review. Atmos. Environ. 262, 118592.

Hewitt, C., 2001. The atmospheric chemistry of sulphur and nitrogen in power station plumes. Atmos. Environ. 35, 1155–1170.

Hristova, E., Veleva, B., Georgieva, E., Branzov, H., 2020. Application of positive matrix factorization receptor model for source identification of PM10 in the city of Sofia. Bulgaria. Atmosphere 11, 890.

In't Veld, M., Alastuey, A., Pandolfi, M., Amato, F., Perez, N., Reche, C., et al., 2021. Compositional changes of PM2. 5 in NE Spain during 2009–2018: a trend analysis of the chemical composition and source apportionment. Sci. Total Environ. 795, 148728.

Ivaneev, A., Brzhezinskiy, A., Karandashev, V., Ermolin, M., Fedotov, P., 2023. Assessment of sources, environmental, ecological, and health risks of potentially toxic elements in urban dust of Moscow megacity. Russia. Chemosphere 321, 138142.

Järvi, L., Junninen, H., Karppinen, A., Hillamo, R., Virkkula, A., Mäkelä, T., et al., 2008. Temporal variations in black carbon concentrations with different time scales in Helsinki during 1996–2005. Atmos. Chem. Phys. 8, 1017–1027.

Karagulian, F., Belis, C.A., 2012. Enhancing source apportionment with receptor models to foster the air quality directive implementation. Int. J. Environ. Pollut. 50, 190–199.

Kasimov, N.S., Kosheleva, N.E., Vlasov, D.V., Nabelkina, K.S., Ryzhov, A.V., 2019. Physicochemical properties of road dust in Moscow. Geography, environment, sustainability 12, 96–113.

Kasimov, N.S., Vlasov, D.V., Kosheleva, N.E., 2020. Enrichment of road dust particles and adjacent environments with metals and metalloids in eastern Moscow. Urban Clim. 32, 100638.

Knippertz, P., Stuut, J.-B.W., 2014. Mineral dust. Mineral dust—a key player in the Earth system 121–147.

Koçak, M., Theodosi, C., Zarmpas, P., Im, U., Bougiatioti, A., Yenigun, O., et al., 2011. Particulate matter (PM10) in Istanbul: origin, source areas and potential impact on surrounding regions. Atmos. Environ. 45, 6891–6900.

Kolesar, K.R., Mattson, C.N., Peterson, P.K., May, N.W., Prendergast, R.K., Pratt, K.A., 2018. Increases in wintertime PM2. 5 sodium and chloride linked to snowfall and road salt application. Atmos. Environ. 177, 195–202.

Kong, S., Ji, Y., Lu, B., Chen, L., Han, B., Li, Z., et al., 2011. Characterization of PM10 source profiles for fugitive dust in Fushun-a city famous for coal. Atmos. Environ. 45, 5351–5365.

Laupsa, H., Denby, B., Larssen, S., Schaug, J., 2007. Source Apportionment of Particulate Matter Using Dispersion and Receptor Modelling. A Case Study for Oslo, NILU OR.

Lokoshchenko, M., Bogdanovich, A.Y., Elansky, N., Lezina, Y.A., 2021. Thermal inversions and their influence on the composition of the surface air layer over Moscow. Izvestiya, Atmospheric and Oceanic Physics 57, 559–567.

Ma, Y., Huang, Y., Wu, J., J, E., Zhang, B., Han, D., et al., 2022. A review of atmospheric fine particulate matters: chemical composition, source identification and their variations in Beijing. Energy Sources, Part A 44, 4783–4807.

Manousakas, M., Popovicheva, O., Evangeliou, N., Diapouli, E., Sitnikov, N., Shonija, N., et al., 2020. Aerosol carbonaceous, elemental and ionic composition variability and origin at the Siberian High Arctic, Cape Baranova. Tellus Ser. B Chem. Phys. Meteorol. 72, 1–14.

Masiol, M., Squizzato, S., Formenton, G., Khan, M.B., Hopke, P.K., Nenes, A., et al., 2020. Hybrid multiple-site mass closure and source apportionment of PM2. 5 and aerosol acidity at major cities in the Po Valley. Sci. Total Environ. 704, 135287.

Molnár, P., Tang, L., Sjöberg, K., Wichmann, J., 2017. Long-range transport clusters and positive matrix factorization source apportionment for investigating transboundary PM 2.5 in Gothenburg, Sweden. Environ Sci Process Impacts 19, 1270–1277.

Nava, S., Lucarelli, F., Amato, F., Becagli, S., Calzolai, G., Chiari, M., et al., 2015. Biomass burning contributions estimated by synergistic coupling of daily and hourly aerosol composition records. Sci. Total Environ. 511, 11–20.

Norris, G., Duvall, R., Brown, S., Bai, S., 2014. EPA positive matrix factorization (PMF) 5.0 fundamentals and user guide. In: US Environmental Protection Agency. National Expo Res Lab Res Triangle Park, Petaluma, pp. 1–136.

Padoan, S., Zappi, A., Adam, T., Melucci, D., Gambaro, A., Formenton, G., et al., 2020. Organic molecular markers and source contributions in a polluted municipality of north-East Italy: extended PCA-PMF statistical approach. Environ. Res. 186, 109587.
Pernigotti, D., Belis, C.A., Spano, L., 2016. SPECIEUROPE: the European data base for PM source profiles. Atmos. Pollut. Res. 7, 307–314.
Perrone, M., Vratolis, S., Georgieva, E., Török, S., Šega, K., Veleva, B., et al., 2018. Sources and geographic origin of particulate matter in urban areas of the Danube macro-region: the cases of Zagreb (Croatia), Budapest (Hungary) and Sofia (Bulgaria). Sci. Total Environ. 619, 1515–1529.
Pio, C., Cerqueira, M., Harrison, R.M., Nunes, T., Mirante, F., Alves, C., et al., 2011. OC/EC ratio observations in Europe: re-thinking the approach for apportionment between primary and secondary organic carbon. Atmos. Environ. 45, 6121–6132.
Plaza, J., Artíñano, B., Salvador, P., Gómez-Moreno, F.J., Pujadas, M., Pio, C.A., 2011. Short-term secondary organic carbon estimations with a modified OC/EC primary ratio method at a suburban site in Madrid (Spain). Atmos. Environ. 45, 2496–2506.
Popovicheva, O.B., Engling, G., Diapouli, E., Saraga, D., Persiantseva, N.M., Timofeev, M. A., et al., 2016. Impact of smoke intensity on size-resolved aerosol composition and microstructure during the biomass burning season in Northwest Vietnam. Aerosol Air Qual. Res. 16, 2635–3654.
Popovicheva, O., Diapouli, E., Makshtas, A., Shonija, N., Manousakas, M., Saraga, D., et al., 2019a. East Siberian Arctic background and black carbon polluted aerosols at HMO Tiksi. Sci. Total Environ. 655, 924–938.
Popovicheva, O.B., Engling, G., Ku, I.-T., Timofeev, M.A., Shonija, N.K., 2019b. Aerosol emissions from long-lasting smoldering of boreal peatlands: chemical composition, markers, and microstructure. Aerosol Air Qual. Res. 19, 484–503.
Popovicheva, O., Ivanov, A., Vojtisek, M., 2020c. Functional factors of biomass burning contribution to spring aerosol composition in a megacity: combined FTIR-PCA analyses. Atmosphere 11, 319.
Popovicheva, O., Kistler, M., Kireeva, E., Persiantseva, N., Timofeev, M., Kopeikin, V., Kasper-Giebl, A., 2014. Physicochemical characterization of smoke aerosol during large-scale wildfires: Extreme event of August 2010 in Moscow Atmospheric Environment 96, 405–414.
Popovicheva, O., Padoan, S., Schnelle-Kreis, J., Nguyen, D.-L., Adam, T., Kistler, M., Steinkogler, T., Kasper-Giebl, A., Zimmermann, R., Chubarova, N., 2020b. Spring aerosol in the urban atmosphere of a megacity: analytical and statistical assessment for source impacts. Aerosol Air Qual. Res. 20, 702–719.
Popovicheva, O.B., Volpert, E., Sitnikov, N.M., Chichaeva, M.A., Padoan, S., 2020a. Black carbon in spring aerosols of Moscow urban background. Geography, Environment, Sustainability 13, 233–243.
Popovicheva, O., Chichaeva, M., Kovach, R., Zhdanova, E., Kasimov, N., 2022. Seasonal, weekly, and diurnal black carbon in Moscow megacity background under impact of urban and regional sources. Atmosphere 13, 563.
Putaud, J.-P., Van Dingenen, R., Alastuey, A., Bauer, H., Birmili, W., Cyrys, J., et al., 2010. A European aerosol phenomenology–3: physical and chemical characteristics of particulate matter from 60 rural, urban, and kerbside sites across Europe. Atmos. Environ. 44, 1308–1320.
Querol, X., Alastuey, A., Viana, M.M., Rodriguez, S., Artíñano, B., Salvador, P., et al., 2004. Speciation and origin of PM10 and PM2. 5 in Spain. J. Aerosol Sci. 35, 1151–1172.
Rudnick, R.L., Gao, S., 2014. Composition of the continental crust. In: Treatise on Geochemistry. Elsevier, pp. 1–51.
Rudnick, R., Gao, S., Holland, H., Turekian, K., 2003. Composition of the continental crust. The crust 3, 1–64.
Samonova, O.A., Aseyeva, E.N., Chernitsova, O.V., 2020. Data on rare earth elements in different particle size fractions of topsoil for two small erosional landforms in central European Russia. Data Brief 30, 105450.
Saraga, D., Maggos, T., Degrendele, C., Klánová, J., Horvat, M., Kocman, D., Kanduč, T., Dos Santos, S.G., Franco, R., Morillo Gómez, P., Manousakas, M., Bairachtari, K., Eleftheriadis, K., Kermenidou, M., Karakitsios, S., Gotti, A., Sarigiannis, D., 2021. Multi-citycomparative PM2.5 source apportionment for fifteen sites in Europe: The ICARUS project. Sci. Total Environ. 751, 141855.
Seinfeld, J.H., Pandis, S.N., 2016. Atmospheric Chemistry and Physics: From Air Pollution to Climate Change. John Wiley & Sons.
Sharma, S., Mandal, T., Saxena, M., Sharma, A., Gautam, R., 2014. Source apportionment of PM10 by using positive matrix factorization at an urban site of Delhi. India. Urban climate 10, 656–670.
Stein, A., Draxler, R., Rolph, G., Stunder, B., Cohen, M., Ngan, F., 2015. NOAA's HYSPLIT atmospheric transport and dispersion modeling system. B. Am. Meteorol. Soc. 96, 2059–2077.
Stieger, B., Spindler, G., Fahlbusch, B., Müller, K., Grüner, A., Poulain, L., et al., 2018. Measurements of PM 10 ions and trace gases with the online system MARGA at the research station Melpitz in Germany–a five-year study. J. Atmos. Chem. 75, 33–70.
Thunis, P., Clappier, A., Pirovano, G., 2020. Source Apportionment to Support Air Quality Management Practices: A Fitness-for-Purpose Guide V3. 1. Union européenne.
Tositti, L., Brattich, E., Masiol, M., Baldacci, D., Ceccato, D., Parmeggiani, S., et al., 2014. Source apportionment of particulate matter in a large city of southeastern Po Valley (Bologna, Italy). Environ. Sci. Pollut. Res. 21, 872–890.
Viana, M., Kuhlbusch, T.A., Querol, X., Alastuey, A., Harrison, R.M., Hopke, P.K., et al., 2008. Source apportionment of particulate matter in Europe: a review of methods and results. J. Aerosol Sci. 39, 827–849.
Vlasov, D., Kosheleva, N., Kasimov, N., 2021. Spatial distribution and sources of potentially toxic elements in road dust and its PM10 fraction of Moscow megacity. Sci. Total Environ. 761, 143267.
Vlasov, D.V., Vasil'chuk, J.Y., Kosheleva, N.E., Kasimov, N.S., 2023. Contamination levels and source apportionment of potentially toxic elements in size-fractionated road dust of Moscow. Environ. Sci. Pollut. Res. 30, 38099–38120.
Waked, A., Favez, O., Alleman, L., Piot, C., Petit, J.-E., Delaunay, T., et al., 2014. Source apportionment of PM 10 in a north-western Europe regional urban background site (Lens, France) using positive matrix factorization and including primary biogenic emissions. Atmos. Chem. Phys. 14, 3325–3346.
Watson, J.G., Antony Chen, L.-W., Chow, J.C., Doraiswamy, P., Lowenthal, D.H., 2008. Source apportionment: findings from the US supersites program. J. Air Waste Manage. Assoc. 58, 265–288.
Yang, D., Li, Z., Yue, Z., Liu, J., Zhai, Z., Li, Z., et al., 2022. Variations in sources, composition, and exposure risks of PM2. 5 in both pre-heating and heating seasons. Aerosol Air Qual. Res. 22, 210333.
Yttri, K.E., Simpson, D., Stenström, K., Puxbaum, H., Svendby, T., 2011. Source apportionment of the carbonaceous aerosol in Norway–quantitative estimates based on 14 C, thermal-optical and organic tracer analysis. Atmos. Chem. Phys. 11, 9375–9394.
Zappi, A., Popovicheva, O., Tositti, L., Chichaeva, M., Eremina, I., Kasper-Giebl, A., et al., 2023. Factors influencing aerosol and precipitation ion chemistry in urban background of Moscow megacity. Atmos. Environ. 294, 119458.
Zhang, R., Jing, J., Tao, J., Hsu, S.C., Wang, G., Cao, J., et al., 2013. Chemical characterization and source apportionment of $PM_{2.5}$ in Beijing: seasonal perspective. Atmos. Chem. Phys. 13, 7053–7074.
Zhdanova, E.Y., Chubarova, N.Y., Lyapustin, A.I., 2020. Assessment of urban aerosol pollution over the Moscow megacity by the MAIAC aerosol product. Atmos. Meas. Tech. 13, 877–891.
Zhu, Y., Huang, L., Li, J., Ying, Q., Zhang, H., Liu, X., et al., 2018. Sources of particulate matter in China: insights from source apportionment studies published in 1987–2017. Environ. Int. 115, 343–357.